

1  
2  
3  
4  
5  
6  
7  
8  
9  
10  
11  
12  
13  
14  
15  
16  
17  
18  
19  
20  
21  
22  
23

## Leaf Wax Hydrogen Isotopes as a Hydroclimate Proxy in the Tropical Pacific

S. N. Ladd<sup>1,2\*</sup>, A. E. Maloney<sup>3,4</sup>, D. B. Nelson<sup>5</sup>, M. Prebble<sup>6,7</sup>, G. Camperio<sup>1,2</sup>, D. A. Sear<sup>8</sup>, J. D. Hassall<sup>8</sup>, P. G. Langdon<sup>8</sup>, J. P. Sachs<sup>3</sup>, and N. Dubois<sup>1,2</sup>

<sup>1</sup>Swiss Federal Institute of Aquatic Science and Technology (EAWAG), Dept. of Surface Waters – Research and Management, Dübendorf, CH. <sup>2</sup>Swiss Federal Institute of Technology (ETH-Zürich), Dept. of Earth Sciences, Zürich, CH. <sup>3</sup>University of Washington, School of Oceanography, Seattle, USA. <sup>4</sup>Princeton University, Dept. of Geosciences, Princeton, USA. <sup>5</sup>University of Basel, Dept. of Environmental Sciences-Botany, Basel, CH. <sup>6</sup>University of Canterbury, School of Earth and Environment, Christchurch, NZ. <sup>7</sup>Australian National University, School of Culture, History and Languages, Canberra, AU. <sup>8</sup>University of Southampton, School of Geography and Environmental Science, Southampton, UK.

Corresponding author: S. Nemiah Ladd ([nemiah.ladd@cep.uni-freiburg.de](mailto:nemiah.ladd@cep.uni-freiburg.de))

\*Current address: University of Freiburg, Ecosystem Physiology, Freiburg, DE

### Key Points:

- Leaf wax <sup>2</sup>H/<sup>1</sup>H ratios are correlated with mean annual precipitation <sup>2</sup>H/<sup>1</sup>H ratios globally, but not in the tropical Pacific
- Deviations from the global relationship between precipitation leaf wax <sup>2</sup>H/<sup>1</sup>H ratios cannot be predicted from palynological assemblages
- Small range and large uncertainties in estimates of tropical Pacific precipitation <sup>2</sup>H/<sup>1</sup>H ratios likely account for poor correlations

**Abstract**

Hydrogen isotope ratios of sedimentary leaf waxes ( $\delta^2\text{H}_{\text{Wax}}$  values) are increasingly used to reconstruct past hydroclimate. Here, we add  $\delta^2\text{H}_{\text{Wax}}$  values from 19 lakes and four swamps on 15 tropical Pacific islands to an updated global compilation of published data from surface sediments and soils. Globally, there is a strong positive linear correlation between  $\delta^2\text{H}$  values of mean annual precipitation ( $\delta^2\text{H}_{\text{P}}$  values) and the leaf waxes *n*-C<sub>29</sub>-alkane ( $R^2 = 0.74$ ,  $n = 665$ ) and *n*-C<sub>28</sub>-acid ( $R^2 = 0.74$ ,  $n = 242$ ). Tropical Pacific  $\delta^2\text{H}_{\text{Wax}}$  values fall within the predicted range of values based on the global calibration, and the largest residuals from the global regression line are no greater than those observed elsewhere, despite large uncertainties in  $\delta^2\text{H}_{\text{P}}$  values at some Pacific sites. However, tropical Pacific  $\delta^2\text{H}_{\text{Wax}}$  values in isolation are not correlated with estimated  $\delta^2\text{H}_{\text{P}}$  values from isoscapes or from isotope-enabled general circulation models. Palynological analyses from these same Pacific sediment samples suggest no systematic relationship between any particular type of pollen distribution and deviations from the global calibration line. Rather, the poor correlations observed in the tropical Pacific are likely a function of the small range of  $\delta^2\text{H}_{\text{P}}$  values relative to the typical residuals around the global calibration line. Our results suggest that  $\delta^2\text{H}_{\text{Wax}}$  values are currently most suitable for use in detecting large changes in precipitation in the tropical Pacific and elsewhere, but that ample room for improving this threshold exists in both improved understanding of  $\delta^2\text{H}$  variability in plants, as well as in precipitation.

43

**Plain Language Summary**

Past precipitation patterns are difficult to reconstruct, limiting our ability to understand Earth's climate system. Geochemists reconstruct past precipitation by measuring the amount of

47 heavy hydrogen naturally incorporated into the waxy coating of leaves, which is preserved in  
48 mud that accumulates in lakes, soils, and oceans. Heavy hydrogen in leaf waxes is strongly  
49 correlated with local precipitation, allowing us to learn about rainfall intensity, temperature, and  
50 cloud movement. However, no existing calibration studies include sites from the tropical Pacific,  
51 home to the most intense rainfall on the planet and populations that rely on rain for drinking  
52 water. We measured heavy hydrogen in leaf waxes from tropical Pacific islands and show that  
53 although values are within the global calibration error, no precipitation relationship exists within  
54 the region. Plant type distributions do not explain the lack of correlation, which is best attributed  
55 to poorly constrained estimates of heavy hydrogen in local rain and the relatively small range of  
56 variability within the region. At present, heavy hydrogen from ancient leaf waxes can show large  
57 changes in past precipitation, but improved process-level understanding is needed to use this tool  
58 to understand smaller changes in the tropical Pacific and elsewhere.

## 59 **1 Introduction**

60 As Earth warms, precipitation intensity, frequency, and spatial distribution are expected to  
61 change over the tropical Pacific (Brown et al., 2011; Tan et al., 2015; Sharmila et al., 2018).  
62 These predictions need to be constrained and validated by robust reconstructions of past changes,  
63 which are unfortunately limited in this region, in part because of a lack of proxies and archives  
64 suitable for producing high resolution, continuous records (Hassall 2017). Existing high-  
65 resolution paleohydrologic records have been established from speleothems (Partin et al., 2013;  
66 Maupin et al., 2014) and corals (Quinn et al., 1993; Quinn et al., 1998; Hendy et al, 2002;  
67 Linsley et al., 2004; Linsley et al., 2006; Calvo et al., 2007; DeLong et al., 2012), but are  
68 generally limited to the past 600 years in this region. Lacustrine and swamp sediments can  
69 provide longer records with much higher temporal resolution than is possible from slowly

70 accumulating marine sediments, and are well-established archives of ecological, anthropogenic,  
71 and broad climatic changes in the region (Southern, 1986; Hope & Pask, 1998; Stevenson et al.,  
72 2001; Prebble & Wilmshurst, 2009; Prebble et al., 2019; Gosling et al., 2020). More recently,  
73 such sediments have also been used to reconstruct past hydroclimate change in the western  
74 tropical Pacific at higher temporal resolution (Sachs et al., 2009; Smittenburg et al., 2011;  
75 Konecky et al., 2016; Richey & Sachs, 2016; Hassall, 2017; Sachs et al., 2018; Sear et al., 2020).

76 One hydroclimate proxy suitable for tropical lake and swamp sediments in the tropical  
77 Pacific is based on the hydrogen isotopic composition of leaf waxes ( $\delta^2\text{H}_{\text{Wax}} =$   
78  $(^2\text{H}/^1\text{H})_{\text{Wax}} / (^2\text{H}/^1\text{H})_{\text{VSMOW}} - 1$ ) (Sachse et al., 2012; Konecky et al., 2016; Hassall, 2017).  $\delta^2\text{H}_{\text{Wax}}$   
79 values are highly correlated with hydrogen isotopes of mean annual precipitation ( $\delta^2\text{H}_{\text{P}}$ ) on a  
80 global scale and have been applied to reconstruct  $\delta^2\text{H}_{\text{P}}$  values in diverse locations (Sachse et al.,  
81 2012; McFarlin et al., 2019).  $\delta^2\text{H}_{\text{P}}$  values are related to specific physical processes, and are a  
82 chemical signal that can both be transferred to material preserved on geologic timescales, as well  
83 as modeled in modern systems with increasing accuracy, making their reconstructions useful for  
84 understanding past hydroclimate dynamics (Bowen et al., 2019).

85 As is typical for organic geochemical proxies, the relationship between  $\delta^2\text{H}_{\text{Wax}}$  and  $\delta^2\text{H}_{\text{P}}$   
86 has been established through empirical calibrations with surface sediments from lakes and  
87 surface soils. These calibration efforts began in Europe (e.g., Sachse et al., 2004; Leider et al.,  
88 2013; Nelson et al., 2018) and have been extended to the Americas (e.g., Hou et al., 2008;  
89 Polissar & Freeman, 2010; Douglas et al., 2013), East Asia and the Tibetan Plateau (e.g., Jia et  
90 al., 2008; Aichner et al., 2010; Bai et al., 2011), and Africa (e.g., Peterse et al., 2009; Garcin et  
91 al., 2012; Schwab et al., 2015) (Figure 1). Recent compilations of  $\delta^2\text{H}_{\text{Wax}}$  from surface sediments  
92 (McFarlin et al., 2019) and from sediments and soils (Liu & An, 2019) placed these local

93 calibrations in a global context. However, existing global compilations do not include any  
94 tropical Pacific  $\delta^2\text{H}_{\text{Wax}}$  values.

95 Two considerations make it important to include tropical Pacific data in the global  
96 calibration. Firstly, different vegetation types can influence net community  $^2\text{H}/^1\text{H}$  fractionation  
97 between precipitation and leaf waxes, which is not constant among plant types or environments  
98 (Feakins and Sessions, 2010; Sachse et al., 2012; Kahmen et al., 2013). The unique plant  
99 communities on tropical Pacific islands include many endemic species (Gillespie et al., 2013).  
100 Additionally, coastal regions or former lagoons on these islands are often covered by mangrove  
101 swamps, which consist of trees and shrubs adapted to brackish to hypersaline water. Due to  
102 salinity effects, mangrove  $\delta^2\text{H}_{\text{Wax}}$  values may have the opposite response to changes in  
103 precipitation intensity as nearby freshwater plants (Ladd & Sachs, 2012; He et al., 2017).  
104 However, the impact of mangrove contributions to sedimentary  $\delta^2\text{H}_{\text{Wax}}$  values has not been  
105 assessed.

106 Secondly, there is large uncertainty associated with estimates of  $\delta^2\text{H}_\text{P}$  in the tropical  
107 Pacific. Direct measurements of  $\delta^2\text{H}_\text{P}$  from the Global Network of Isotopes in Precipitation  
108 (GNIP) are spatially and temporally limited compared to other regions, resulting in large  
109 uncertainties for statistical interpolations of  $\delta^2\text{H}_\text{P}$  such as those used for isoscape products and  
110 the Online Isotopes in Precipitation Calculator (OIPC; Bowen & Revenaugh, 2003). Estimates of  
111  $\delta^2\text{H}_\text{P}$  from general circulation models (GCMs) in which precipitation isotopes have been  
112 incorporated offer another potential calibration target for  $\delta^2\text{H}_{\text{Wax}}$  measurements in the modern  
113 tropical Pacific that has not yet been explored.

114 Here we measured  $\delta^2\text{H}$  values of seven *n*-alkane and five *n*-alkanoic acid homologues from  
115 surface sediments collected from lakes influenced by precipitation from the South Pacific  
116 Convergence Zone (SPCZ) and from mangrove swamps influenced by the Intertropical

117 Convergence Zone (ITCZ). We add new surface sediment  $\delta^2\text{H}_{\text{Wax}}$  measurements of two of these  
118 compounds (*n*-C<sub>29</sub>-alkane and *n*-C<sub>28</sub>-acid) from 19 lakes and four mangrove swamps on 15  
119 islands distributed throughout the tropical Pacific to an updated global compilation of  $\delta^2\text{H}_{\text{Wax}}$   
120 values. We assess whether  $\delta^2\text{H}_{\text{Wax}}$  values from tropical Pacific lake and swamp sediments are  
121 consistent with the global relationship between  $\delta^2\text{H}_{\text{Wax}}$  and modeled  $\delta^2\text{H}_\text{P}$  values from a diverse  
122 set of algorithms and models. Finally, we use pollen-based vegetation reconstructions to evaluate  
123 the influence of plant communities on tropical Pacific  $\delta^2\text{H}_{\text{Wax}}$  values.

## 124 **2 Materials and Methods**

### 125 2.1 Site description and sample collection

126 Surface sediments were collected from 19 lakes on 11 islands across the SPCZ region  
127 (Figure 1, Table 1), ranging in elevation above mean sea level from 790 m (Lanoto'o, Samoa) to  
128 1 m (Rimatu'u, Oroatera, and Onetahi ponds on Tetiaroa, French Polynesia). Lakes ranged from  
129 shallow ephemeral water bodies to an 88 m-deep volcanic crater lake (Lake Lalolalo, Wallis).  
130 Most lakes were freshwater systems, except for the brackish (salinity = 17) coastal Lake  
131 Dranoniveilomo (Fiji) and Lake Lalolalo (Wallis), which has a freshwater surface lens above  
132 saline water (Sichrowsky et al., 2014). Mangrove trees surrounded Lake Dranoniveilomo, while  
133 many other sites were located in forested regions, some impacted by human activity, particularly  
134 horticulture. Aquatic vegetation covered the surface of some lakes (Table 1). Additional samples  
135 were obtained from mangrove swamps located within the ITCZ throughout the Federated States  
136 of Micronesia and Guam. All swamps were located at sea level and submerged at high tide. Four  
137 or five surface sediment samples were collected from each swamp along a transect from the  
138 inland edge to the coast.

139 Maloney et al. (2019) described the collection of most lake samples from the SPCZ region.  
140 New samples include those from Lake Dranoniveilomo, which was cored in 2010 with a  
141 Universal Percussion Corer (Aquatic Research, Hope ID, USA) fitted with a 6.6 cm diameter  
142 polycarbonate core tube. Vesalea and Nopovois were cored in 2017 with a percussion corer  
143 (UWITEC, Mondsee, Austria) equipped with a 6.3 cm diameter polycarbonate tube.  
144 Unconsolidated upper sediment from these cores was subsampled at 1 cm intervals in the field  
145 and stored frozen in Whirl-Pak plastic bags (Nasco, Fort Atkinson, WI, USA). Analyses of lake  
146 surface sediment were restricted to the uppermost 1 or 2 cm of material. A hand trowel was used  
147 to collect the upper 1 cm of mangrove sediments in 2012. Samples were stored frozen in Whirl-  
148 Pak bags.

149 Water was collected from the surface of each lake and stored in screw-cap glass vials.  
150 Additional water samples were collected from adjacent streams and long-term precipitation  
151 integrators such as wells and rain cisterns when available. Samples were stored at 4 °C prior to  
152 analysis.

153

## 154 2.2 Leaf wax extraction and purification

155 Maloney et al. (2019) described lipid extraction, saponification, and column  
156 chromatography for all lake surface sediments except Dranoniveilomo, Vesalea, and Nopovois.  
157 Samples from Dranoniveilomo were processed following the protocol of Maloney et al. (2019).  
158 For all these lake sediments, the acid-containing fraction was eluted with 6 ml 4% acetic acid in  
159 diethyl ether from an aminopropyl gel column and the alkane-containing fraction was eluted with  
160 6 ml hexane from a silica gel column. Lipid extraction, saponification, and column  
161 chromatography from Vesalea was described by Krentscher et al. (2019), and was identical for

162 the sample from Nopovois. Lipids from mangrove surface sediments were extracted and divided  
163 into compound classes using Si gel column chromatography as in Ladd and Sachs (2017).

164 For mangrove surface sediments, *n*-alkanes were purified from a Si gel hexane fraction by  
165 eluting 8 mL of 100% hexane over 0.5 g of AgNO<sub>3</sub>-impregnated Si gel (10% by weight). For  
166 lake samples, the alkane fraction was urea adducted to isolate unbranched compounds. Fatty  
167 acids from lake sediments were methylated with 5% HCl in methanol for 12 hours at 70 °C, and  
168 saturated fatty acid methyl esters (FAMES) were isolated by elution in 8 mL of 4:1 Hex/DCM  
169 over 0.5 g of AgNO<sub>3</sub>-impregnated Si gel (10% by weight). Acid fractions were not analyzed  
170 from mangrove surface sediments. Purity and concentrations of *n*-alkanes from mangrove  
171 samples were assessed by gas chromatography – flame ionization detection (GC-FID) using the  
172 GC program and instrumentation described in Ladd and Sachs (2017). For lake samples, *n*-  
173 alkane and *n*-acid homologues were quantified using the same GC program and instrumentation  
174 described in Ladd et al. (2018).

175

### 176 2.3 $\delta^2\text{H}_{\text{Wax}}$ measurements

177 Samples were dissolved in hexane at a concentration suitable for hydrogen isotope  
178 analyses of *n*-C<sub>29</sub>-alkane or *n*-C<sub>28</sub>-acid when those compounds were sufficiently abundant for  
179 analysis by gas chromatography – isotope ratio mass spectrometry (GC-IRMS).  $\delta^2\text{H}$  values of  
180 other baseline-resolved homologues with peak areas >15 Vs are also reported. For mangrove  
181 sediment samples, GC-IRMS analyses were conducted with the same GC program and isotopic  
182 referencing described in Ladd and Sachs (2017). Lake sediment samples were analyzed with the  
183 same GC program and isotopic referencing described in Ladd et al. (2018). Phthalic acid of  
184 known isotopic composition (Shimmelmann, Indiana University) was methylated to determine

185  $\delta^2\text{H}$  values of H added during methylation, which was corrected for using isotopic mass balance  
186 (Lee et al., 2017).

187

#### 188 2.4 Estimates of $\delta^2\text{H}_p$ values

189 Estimates of  $\delta^2\text{H}_p$  values were extracted from different model products using latitude,  
190 longitude, and elevation of each site. Model products included the Online Isotopes in  
191 Precipitation Calculator (OIPC) version 3.2 (Bowen & Ravenaugh, 2003; IAEA/WMO, 2015;  
192 Bowen, 2020), as well as isotope-enabled climate model contributions to the second Stable  
193 Water Isotope Intercomparison Group (SWING2) from the CAM, ECHAM, GISS ModelE,  
194 HadAM, isoGSM, LMDZ, and MIROC models (Sturm et al., 2010). OIPC estimated values were  
195 obtained manually from the web interface (“OIPC mean annual  $\delta^2\text{H}$ ”), and also by extraction  
196 from the high-resolution spatial gridded data set using a bilinear smooth function to  
197 accommodate the proximity of a given location to neighboring pixels and the  $\delta^2\text{H}$  values from  
198 those pixels (“OIPC extracted mean annual  $\delta^2\text{H}$ ”). The multi-model mean annual precipitation  
199  $\delta^2\text{H}$  value was calculated by averaging predicted values for all climate models that employed  
200 spectral nudging (Yoshimura et al., 2008), which includes the ECHAM, GISS (nudged),  
201 isoGSM, and LMDZ products.

202

#### 203 2.5 Water $\delta^2\text{H}$ and $\delta^{18}\text{O}$ analyses

204 The isotopic composition of most lake and stream water samples were previously  
205 analyzed and reported by Maloney et al. (2019). Water samples from the 2012 Micronesian field  
206 campaign and from Lake Dranoniveilomo were analyzed by Cavity Ring Down Spectroscopy  
207 (CRDS; Li-2130i, Picarro, Santa Clara, CA) using the same conditions and standards as in  
208 Maloney et al. (2019). Additional water samples from the 2017 Vanuatu field campaign were

209 analyzed by Thermal Conversion/Elemental Analysis – Isotope Ratio Mass Spectrometry  
210 (TC/EA-IRMS; ThermoFisher Scientific, Bremen, Germany) using the same conditions and  
211 standards as in Newberry et al. (2017).

212

## 213 2.6 Pollen counts

214 Core samples for palynomorph analyses (including pollen and spores) were taken from  
215 within the upper portion of the sediment core to determine modern baseline vegetation  
216 differences among lakes. Each 1 cm<sup>3</sup> sample was processed using standard procedures (10%  
217 HCl, hot 10% KOH, and acetolysis) (Moore et al. 1991). Samples were spiked with exotic  
218 *Lycopodium clavatum* L. tablets to allow the palynomorph and charcoal concentrations to be  
219 calculated. Counts continued until reaching at least 100 terrestrial palynomorphs. Reference  
220 palynomorphs held in the Australasian Pollen and Spore Atlas ([apsa.anu.edu.au/](http://apsa.anu.edu.au/)) assisted with  
221 identification. The vegetation types (primary, secondary, dryland herbs, wetland herbs, etc.) were  
222 determined from a regional synthesis of Pacific Island plant ecology (Mueller-Dombois &  
223 Fosberg 1998).

## 224 **3 Results**

### 225 3.1 $\delta^2\text{H}_{\text{Wax}}$ values in the tropical Pacific

226  $\delta^2\text{H}_{\text{Wax}}$  values from surface sediments in the tropical Pacific were not correlated with mean  
227 annual  $\delta^2\text{H}_\text{P}$  values as calculated by the OIPC, nor with mean annual precipitation amount as  
228 estimated by the Global Precipitation Climatology Project (GPCP) (Adler et al., 2003) (Figure  
229 2). The only lipids with significant correlations with  $\delta^2\text{H}_\text{P}$  values were dinosterol (data from  
230 Maloney et al., 2019), *n*-C<sub>16</sub>-acid, and *n*-C<sub>18</sub>-acid, and the only significant correlations with the  
231 amount of mean annual precipitation were dinosterol, *n*-C<sub>18</sub>-acid, *n*-C<sub>17</sub>-alkane, and *n*-C<sub>33</sub>-alkane.

232 In almost all cases, correlation coefficients were negative for the relationship between  $\delta^2\text{H}_{\text{Wax}}$   
233 and  $\delta^2\text{H}_{\text{P}}$  values, and positive for the relationship between  $\delta^2\text{H}_{\text{Wax}}$  values and mean annual  
234 precipitation. An exception was *n*-C<sub>17</sub>-alkane, which, similarly to dinosterol, had  $\delta^2\text{H}$  values that  
235 are negatively correlated with mean annual precipitation ( $R = -0.95$ ;  $p = 0.049$ ) and positively  
236 correlated with  $\delta^2\text{H}_{\text{P}}$  values ( $R = 0.95$ ;  $p = 0.051$ ) (Figure 2). However, *n*-C<sub>17</sub>-alkane was only  
237 abundant enough to measure its  $\delta^2\text{H}$  values in four samples, making any assessment of these  
238 correlations tentative.

239

### 240 3.2 Tropical Pacific $\delta^2\text{H}$ values in the global context

241 Tropical Pacific  $\delta^2\text{H}$  values of *n*-C<sub>29</sub>-alkanes and *n*-C<sub>28</sub>-acids (the most commonly  
242 measured leaf waxes in the literature) were in the range expected based on the global relationship  
243 between  $\delta^2\text{H}_{\text{Wax}}$  and  $\delta^2\text{H}_{\text{P}}$  values (Figure 3). Tropical Pacific *n*-C<sub>29</sub>-alkane  $\delta^2\text{H}$  values ranged  
244 from  $-177$  to  $-139\text{‰}$ , while those of *n*-C<sub>28</sub>-acid ranged from  $-175$  to  $-119\text{‰}$  (Table 1; Figure  
245 3). Adding these new measurements to an updated global compilation of  $\delta^2\text{H}_{\text{Wax}}$  values from all  
246 available surface sediment and soil data sets in non-marine settings (compilations from Liu &  
247 An, 2019 and McFarlin et al., 2019, as well as data sets from Nelson, 2013; Bakkellund et al.,  
248 2018; Feng et al., 2019; Goldsmith et al., 2019; Li et al., 2019; Wu et al., 2019; Lu et al., 2020;  
249 Struck et al., 2020; van der Veen et al., 2020) has minimal impact on the slope, y-intercept, or  
250 correlation coefficients for the global linear regression (Figure 3).

251 To compare new measurements from the tropical Pacific to the relationship defined by  
252 previously published values, we calculated their residual values from the global linear regression  
253 between  $\delta^2\text{H}_{\text{Wax}}$  and  $\delta^2\text{H}_{\text{P}}$  (excluding new tropical Pacific data). At most tropical Pacific  
254 locations, residuals from the global linear regression line were within  $\pm 20\text{‰}$ , but were greater  
255 than this at 5 sites for *n*-C<sub>29</sub>-alkane and 6 sites for *n*-C<sub>28</sub>-acid (Table 1). Only two sites (Lake

256 Tagamaucia in Fiji and White Lake in Vanuatu) had residuals greater than 20‰ for both  
257 compounds.

258 We also contextualized variability in the tropical Pacific data relative to the global data set  
259 by randomly subsampling 17 values from the compiled data 4,000 times and comparing the  
260 correlation coefficient between  $\delta^2\text{H}_{\text{Wax}}$  and  $\delta^2\text{H}_\text{P}$  to the range in  $\delta^2\text{H}_\text{P}$  values (Figure 4). None of  
261 these subsampled data sets had ranges in  $\delta^2\text{H}_\text{P}$  values that were as small as the range in the  
262 tropical Pacific (smallest range for *n*-C<sub>29</sub>-alkane = 59‰, for *n*-C<sub>28</sub>-acid = 118‰), so we  
263 subsampled the compiled data again while restricting the maximum range to 100‰ (1,000  
264 iterations each for the highest, lowest, and middle  $\delta^2\text{H}_\text{P}$  values), 50‰ (200 iterations for each  
265 possible 50‰ range with maximum  $\delta^2\text{H}_\text{P}$  values shifted by 10‰), and 35‰ (100 iterations for  
266 each possible 35‰ range with maximum  $\delta^2\text{H}_\text{P}$  values shifted by 5‰). Correlation coefficients  
267 were typically high (>0.5) when the range of  $\delta^2\text{H}_\text{P}$  values was greater than 100‰, and became  
268 increasingly scattered below this threshold (Figure 4). The relationship between the correlation  
269 coefficient and the range of  $\delta^2\text{H}_\text{P}$  values in the tropical Pacific plotted within the range generated  
270 by random subsets. However, tropical Pacific correlation coefficients for both compounds were  
271 more than one standard deviation below the mean value of random sample sets with a  $\delta^2\text{H}_\text{P}$  range  
272 between 30 and 35‰ ( $0.43 \pm 0.28$  for *n*-C<sub>29</sub>-alkane;  $0.22 \pm 0.41$  for *n*-C<sub>28</sub>-acid) (Figure 4).

273 In addition to the OIPC, several water-isotope-enabled GCMs also provide estimates of  
274 mean annual  $\delta^2\text{H}_\text{P}$  values. We extracted  $\delta^2\text{H}_\text{P}$  values for all sites with surface sediment or soil  
275  $\delta^2\text{H}_{\text{Wax}}$  values from each climate model included in the Stable Water Isotope Intercomparison  
276 Group, Phase 2 (SWING 2) model comparison. For all models, global *n*-C<sub>29</sub>-alkane and *n*-C<sub>28</sub>-  
277 acid  $\delta^2\text{H}$  values were positively correlated with  $\delta^2\text{H}_\text{P}$  estimates (Figure 5). For *n*-C<sub>29</sub>-alkane,  
278  $\delta^2\text{H}_{\text{Wax}}$  values were most highly correlated with  $\delta^2\text{H}_\text{P}$  values obtained manually from the OIPC  
279 ( $R = 0.86$ ). The lowest correlation was with  $\delta^2\text{H}_\text{P}$  values from HadAM ( $R = 0.57$ ) (Figure 5). For

280 *n*-C<sub>28</sub>-acid, global  $\delta^2\text{H}_{\text{Wax}}$  values were most highly correlated with  $\delta^2\text{H}_{\text{P}}$  values extracted from the  
281 CAM model ( $R = 0.91$ ). The lowest correlation was with  $\delta^2\text{H}_{\text{P}}$  values extracted from the high-  
282 resolution spatial gridded OIPC data ( $R = 0.82$ ) (Figure 5). The correlation coefficient obtained  
283 manually from the OIPC ( $R = 0.86$ ) was intermediate among the different models (Figure 5).

284

### 285 3.3 Pollen and spore spectra

286 Palynomorphs from most sites were indicative of human disturbance to the catchment  
287 vegetation, as the dominant pollen types are from secondary forest taxa (Figure 6; Table 2).  
288 When secondary forest vegetation was not most abundant, fern spores contributed more to the  
289 palynomorph sum than any other plant group, except at Lake Hut, where primary forest taxa  
290 were most abundant (Figure 6; Table 2). Although wetland plants covered more than 50% of the  
291 surface water at three lakes (Onetahi Pond, Lake Tagamucia, and Veselea Pond), wetland herbs  
292 and aquatic plants never contributed more than 23% of the observed pollen.

293 Pollen data are only available for three of the five sites where *n*-C<sub>29</sub>-alkane residuals from  
294 the global  $\delta^2\text{H}_{\text{Wax}}$  vs.  $\delta^2\text{H}_{\text{P}}$  relationship were less than  $-20\text{‰}$  (Figure 6). In two of these  
295 (Tagamaucia and White Lake), fern spores were abundant (59% and 39%, respectively) (Figure  
296 6; Table 2). However, at the third site with an *n*-C<sub>29</sub>-alkane residual less than  $-20\text{‰}$  (Lake Hut),  
297 fern spore concentrations were low and primary forest taxa palynomorphs were most abundant  
298 (Figure 6; Table 2). Three sites had *n*-C<sub>28</sub>-acid residuals from the global  $\delta^2\text{H}_{\text{Wax}}$  vs.  $\delta^2\text{H}_{\text{P}}$   
299 relationship less than  $-20\text{‰}$ , of which two have pollen data (Tagamaucia and Dranoniveilomo).  
300 Each of these had a high abundance of ferns and wetland plants (80% and 37%, respectively)  
301 (Figure 6, Table 2). Three sites had *n*-C<sub>28</sub>-acid residuals from the global  $\delta^2\text{H}_{\text{Wax}}$  vs.  $\delta^2\text{H}_{\text{P}}$  relations  
302 that were greater than  $20\text{‰}$  (Figure 6). One of these, White Lake, had relatively high  
303 contributions from ferns. The second, Harai Lake #1, does not have recent pollen data (the most

304 recent pollen sample is from 11 – 12 cm), but historically had high contributions from ferns  
305 (Table 2). The third, Nopovois, is dominated by secondary forest vegetation (54%) and does not  
306 have palynological features that clearly distinguish it from sites where *n*-C<sub>28</sub>-acid  $\delta^2\text{H}$  values  
307 adhere more closely to the global relationship (Figure 6; Table 2). Additionally, some sites with  
308 high contributions from ferns and wetland plants – Harai Lake #3, Lanoto'o, and Lake Otas –  
309 have  $\delta^2\text{H}_{\text{Wax}}$  values close to the global relationship (Figure 6).

#### 310 **4 Discussion**

311 Although the relationship between  $\delta^2\text{H}_{\text{Wax}}$  and  $\delta^2\text{H}_\text{P}$  values lacks any correlation for the  
312 tropical Pacific sites in isolation, the values fall within the global scatter around the linear  
313 regression of compiled literature values from surface sediments and soils (Figure 3; Table 1). In  
314 addition to adding recently published data, our global data set differs from two recent  
315 compilations by excluding marine sediments (in contrast to Liu and An, 2019), and including  
316 both soils and surface sediments (in contrast to McFarlin et al., 2019). Although leaf waxes in  
317 soils and sediments might have different sources and represent different timescales and  
318 catchment areas, there is no significant difference in the relationship between  $\delta^2\text{H}_{\text{Wax}}$  and  $\delta^2\text{H}_\text{P}$   
319 for either compound (Figure 3c and 3d). The similarity between the soil and sediment  
320 compilations suggests that the transit history of leaf waxes from plant to deposition and  
321 subsequent preservation varies as much within archive type as it does between them.

322 The positive linear relationship between  $\delta^2\text{H}_{\text{Wax}}$  and  $\delta^2\text{H}_\text{P}$  values in the global compilation  
323 remains robust, with  $R^2$  values of 0.74 for both *n*-C<sub>29</sub>-alkane ( $n = 665$ ) and *n*-C<sub>28</sub>-acid ( $n = 242$ )  
324 (Figure 3). However, considerable scatter around the regression line exists globally and within  
325 the tropical Pacific. Large residuals are due to both uncertainty in the y-axis (variable  $^2\text{H}/^1\text{H}$   
326 fractionation between leaf waxes and water among plant types and environments, discussed in

327 section 4.1) and in the x-axis (mean annual  $\delta^2\text{H}_\text{P}$  values and the water source used by plants,  
328 discussed in section 4.2).

329

#### 330 4.1 Variable hydrogen isotope fractionation during leaf wax synthesis

331 Although global  $\delta^2\text{H}_{\text{Wax}}$  values are well correlated with  $\delta^2\text{H}_\text{P}$  values of mean annual  
332 precipitation (Figures 3, 5), several well-established factors contribute to variability in the net  
333  $^2\text{H}/^1\text{H}$  fractionation between plant waxes and precipitation ( $\alpha_{\text{Wax-P}}$ ) (Sachse et al., 2012).  
334 Variations in  $\alpha_{\text{Wax-P}}$  occur among plant functional types (Liu et al., 2006), between leaves and  
335 other plant organs (Gamarra & Kahmen, 2015), and with relative humidity (Tipple et al., 2015).  
336 Additionally, biosynthetic fractionation between leaf water and waxes can vary seasonally  
337 (Newberry et al., 2015), with environmental stresses (Ladd & Sachs, 2015), and with changes in  
338 plant metabolism (Cormier et al., 2018). Large differences in  $\alpha_{\text{Wax-P}}$  can also exist among plant  
339 species growing at the same site (Feakins & Sessions, 2010; Sachse et al., 2012; Eley et al.,  
340 2014; He et al., 2020). With the current tropical Pacific data set we can only examine factors that  
341 might relate to differences among different types of plants, and not factors that can occur within  
342 a single plant, such as metabolic state. We examine three plant groups – mangroves, aquatic  
343 plants, and ferns – whose contributions may impact community  $\delta^2\text{H}_{\text{Wax}}$  values. By comparing  
344 pollen distributions and information about surrounding vegetation at each site with the residuals  
345 between  $\delta^2\text{H}_{\text{Wax}}$  values and the global calibration line (Figure 6), we demonstrate that changes in  
346 vegetation inferred from pollen cannot consistently explain anomalous  $\delta^2\text{H}_{\text{Wax}}$  values in tropical  
347 Pacific surface sediments.

348

##### 349 4.1.1 Mangroves

350 Mangroves are woody plants that grow in brackish to hypersaline water. They contribute  
351 large amounts of organic matter to coastal sediments in the tropics and subtropics (Alongi,  
352 2014). Because mangroves discriminate more against  $^2\text{H}$  as salinity increases (Ladd & Sachs,  
353 2012; He et al., 2017; Ladd & Sachs, 2017), they should have lower  $\delta^2\text{H}_{\text{Wax}}$  values than nearby  
354 freshwater plants. This relationship was recently observed in the Florida Everglades, where  
355 mangroves have  $\delta^2\text{H}_{\text{Wax}}$  values  $\sim 50\%$  lighter than those from nearby freshwater trees, despite  
356 equivalent  $\delta^2\text{H}_{\text{P}}$  values (He et al., 2020). Significant contributions of mangrove leaf waxes in  
357 coastal areas in the tropical Pacific could result in sedimentary  $\delta^2\text{H}_{\text{Wax}}$  values that fall below the  
358 global calibration line.

359 Several of the lakes in our calibration set were located in coastal areas, but only one,  
360 Dranoniveilomo, had brackish water and mangroves growing directly in its periphery. In this  
361 lake *n*- $\text{C}_{28}$ -acid is significantly depleted relative to the global calibration, but *n*- $\text{C}_{29}$ -alkane is not  
362 (Table 1). Despite the abundant mangroves around Dranoniveilomo, barely any mangrove pollen  
363 was found in the sediment, which may reflect different transport mechanisms and catchment  
364 areas for leaf waxes and pollen (Table 2). Two coastal lakes in Vanuatu (Otas and Waérowa  
365 East) have the highest amounts of mangrove pollen observed in all examined surface sediments  
366 ( $\sim 15\%$ ; Figure 6; Table 2). In Lake Otas,  $\delta^2\text{H}_{\text{Wax}}$  values are close to the values predicted by the  
367 global relationship (Table 1). In Lake Waérowa East, they are slightly higher than expected  
368 (Table 1), opposite to the expected impact of significant mangrove leaf wax contributions. These  
369 data suggest that mangrove leaf waxes are not an important influence on  $\delta^2\text{H}_{\text{Wax}}$  values in  
370 tropical Pacific lake sediments included in this study.

371 Likewise, Micronesian mangrove swamp surface sediments had  $\delta^2\text{H}_{\text{Wax}}$  values that were  
372 consistent with the global linear regression (Table 1; Figure 3). Additionally, there was little  
373 spatial variability in  $\delta^2\text{H}_{\text{Wax}}$  values throughout each individual mangrove swamp, with  $5\%$

374 standard deviations among samples within a single swamp (Table 1). This homogeneity occurred  
375 even though samples were collected from sites with surface water salinity ranging from 0-31 at  
376 the time of collection. Surface water salinity was dynamic throughout these mangrove swamp  
377 surveys, varying temporally and spatially with tides and rain events. Individual mangrove trees  
378 with large root networks therefore had access to water with a wide range of salinities and may  
379 have opportunistically taken up relatively fresh water that was ultimately used in leaf wax  
380 synthesis. Preferential uptake of fresher water by mangroves has been observed previously  
381 (Santini et al., 2015; Reef et al., 2015), and could result in all mangroves throughout a swamp  
382 using water with similar salinity and isotopic composition, consistent with the surface sediment  
383  $\delta^2\text{H}_{\text{Wax}}$  values observed in transects from Micronesian mangrove swamps.

384

#### 385 4.1.2 Aquatic plants

386 Some of the lakes included in the tropical Pacific survey were partially or completely  
387 covered by floating aquatic vegetation (Table 1). Since aquatic plants at diverse sites tend to  
388 have lower alkane  $\delta^2\text{H}_{\text{Wax}}$  values than nearby terrestrial plants (Chikaraishi & Naraoka, 2003;  
389 Gao et al., 2011; Dion-Kirschner et al., 2020; He et al., 2020), differing relative contributions of  
390 leaf waxes from aquatic plants could also reduce sedimentary  $\delta^2\text{H}_{\text{Wax}}$  values. There are a few  
391 reasons why aquatic plants may have relatively low  $\delta^2\text{H}_{\text{Wax}}$  values. First, when a lake is mostly  
392 covered by water lilies or similar aquatic vegetation, there is a physical barrier to evaporation of  
393 lake water, and it may therefore maintain a  $\delta^2\text{H}$  signal similar to that of precipitation, rather than  
394 becoming enriched in  $^2\text{H}$  due to transpiration, as is the case for leaves exposed to air (Kahmen et  
395 al., 2013; Cernusak et al., 2016). Second, it is possible that aquatic plants may exhibit greater  
396 biosynthetic fractionation between leaf water and leaf lipid. However, existing investigations of

397  $\delta^2\text{H}_{\text{Wax}}$  values in submerged aquatic plants suggest this is only likely at high salinity, while plants  
398 grown in freshwater display similar  $\alpha_{\text{Wax-P}}$  values to other plants (Aichner et al, 2017).

399 High contributions from aquatic plants could explain why  $\delta^2\text{H}_{\text{Wax}}$  values at Tagamaucia in  
400 Fiji, which is covered in floating sedge islands (Southern et al., 1986), were very  $^2\text{H}$ -depleted  
401 relative to the global calibration line (Table 1). However, this relationship was not consistent in  
402 all lakes covered by aquatic plants. For example, Lake Veselea in Vanuatu is completely covered  
403 by mats of aquatic plants (primarily *Persicaria cf. attenuata*, *Salvinia molesta*, and *Calystegia*  
404 *soldanella*), yet  $\delta^2\text{H}_{\text{Wax}}$  values from its sediment fell close to the global calibration line (Table 1).  
405 Additionally, pollen from wetland herbs and aquatic plants is not consistently associated with  
406 large or small residuals from the global calibration line (Figure 6). Aquatic plants may have  
407 minimal influence on sedimentary  $\delta^2\text{H}_{\text{Wax}}$  values because submerged plants are not at risk of  
408 desiccation and therefore have little need for the moisture barrier provided by long-chain leaf  
409 waxes. They therefore tend to have low concentrations of these compounds (Ficken et al., 2000;  
410 Dion-Kirschner et al., 2020; He et al., 2020). Overall, our results suggest that increased presence  
411 of aquatic plants does not unequivocally result in decreased  $\delta^2\text{H}_{\text{Wax}}$  values in tropical Pacific lake  
412 sediments.

413

#### 414 4.1.3 Ferns

415 Assessments of  $\delta^2\text{H}_{\text{Wax}}$  values from ferns are limited, but previous studies show that ferns  
416 have similar  $\alpha_{\text{Wax-P}}$  values to many other plant taxa, including lycopods, gymnosperms, eudicots,  
417 and magnoliids (Gao et al., 2014). We therefore had no expectation that sites with large  
418 sedimentary contributions of leaf waxes from ferns would diverge from the global  $\delta^2\text{H}_{\text{Wax}}-\delta^2\text{H}_{\text{P}}$   
419 linear regression. However, some of the sites with the largest residuals relative to the global  
420 regression line had palynomorph spectra characterized by large contributions of fern spores. This

421 was particularly true at Lake Tagamaucia in Fiji and White Lake in Vanuatu, and to a lesser  
422 extent in Fiji's Lake Dranoniveilomo (Table 1; Figure 6). However, high accumulation of fern  
423 spores did not universally correspond to low  $\delta^2\text{H}_{\text{Wax}}$  values, for example at Lake Lanoto'o in  
424 Samoa and Harai Lakes #1 and #3 in the Solomon Islands (Tables 1 and 3; Figure 6). Of these,  
425 *n*-C<sub>28</sub>-acid  $\delta^2\text{H}$  values from the Harai Lakes were much higher than the predicted values from the  
426 global regression fit, in direct contrast to the Fijian lakes and White Lake (Table 1; Figure 6).  
427 Additionally, Lake Hut in New Caledonia had the largest *n*-C<sub>29</sub>-alkane residual for any site with  
428 pollen data, but did not have much fern pollen (Figure 6). Overall, this suggests that relative  
429 contributions of leaf waxes from ferns do not have predictable effects on sedimentary  $\delta^2\text{H}_{\text{Wax}}$   
430 values. Nevertheless, a shift in  $\delta^2\text{H}_{\text{Wax}}$  values that coincides with a change in the relative  
431 abundance of fern spores in a down-core record may indicate a change in organic matter sources  
432 rather than a change in  $\delta^2\text{H}_{\text{P}}$  values.

433

#### 434 4.2 Uncertainty in $\delta^2\text{H}_{\text{P}}$ values

435 Variability in  $\alpha_{\text{Wax-P}}$  contributes to uncertainty in the y-axis in the relationship between  
436  $\delta^2\text{H}_{\text{Wax}}$  and  $\delta^2\text{H}_{\text{P}}$  (Figure 3). However, unlike most proxy systems, the x-axis calibration target is  
437 poorly constrained and likely accounts for a large portion of the linear regression residuals  
438 between  $\delta^2\text{H}_{\text{Wax}}$  and  $\delta^2\text{H}_{\text{P}}$  values in the tropical Pacific.  $\delta^2\text{H}_{\text{P}}$  values are not constant throughout  
439 the year, and water from different seasons has different residence times in soil, meaning that the  
440  $\delta^2\text{H}$  values of water used by plants is typically not equal to mean annual  $\delta^2\text{H}_{\text{P}}$  values (Brinkmann  
441 et al., 2018). Additionally,  $\delta^2\text{H}_{\text{P}}$  values from the OIPC represent climatological means, but  $\delta^2\text{H}_{\text{P}}$   
442 values vary interannually and seasonally. The time period captured by a surface sediment sample  
443 (typically a few years to two decades; see Maloney et al., 2019 for sediment accumulation rates  
444 at most sites) may differ considerably from the long-term mean. Finally, the robustness of mean

445 annual estimates provided by the OIPC varies spatially among geographic settings due to the  
446 uneven density of  $\delta^2\text{H}_\text{P}$  observations (IAEA/WMO, 2015).

447 Limited  $\delta^2\text{H}_\text{P}$  data from some sites in the tropical Pacific mean that  $\delta^2\text{H}_\text{P}$  values calculated  
448 using OIPC have large uncertainties (Table 1). This is especially problematic for sites in the  
449 southeastern portion of the region, since there are no observations of  $\delta^2\text{H}_\text{P}$  values from the  
450 Solomon Islands, Vanuatu, or New Caledonia in the GNIP database. 95% confidence intervals  
451 for  $\delta^2\text{H}_\text{P}$  values from sites in Vanuatu are as large as 76‰, considerably larger than the overall  
452 range in  $\delta^2\text{H}_\text{P}$  values (~30‰) and the range in measured  $\delta^2\text{H}_{\text{Wax}}$  values (~40‰ for *n*-C<sub>29</sub>-alkane  
453 and ~55‰ for *n*-C<sub>28</sub>-acid) in the Pacific (Table 1; Figure 3). For other sites, such as those in  
454 Micronesia, OIPC uncertainties may add false confidence to predicted values, as these can be  
455 based on a limited number of GNIP observations from several decades ago. For example, the  
456 Yap GNIP station has 65 observations collected from 1968 to 1976, and the station on Chuuk  
457 (Truk) has 72 observations collected between 1968 and 1977 (IAEA/WMO, 2015).

458 Climatological means calculated from these data may not be representative of conditions when  
459 surface sediment leaf waxes in this study formed. This uncertainty in the independent variable  
460 likely contributes to the lack of a regional correlation between  $\delta^2\text{H}_{\text{Wax}}$  and  $\delta^2\text{H}_\text{P}$  values (Figure 3).

461 An alternative approach for estimating mean annual  $\delta^2\text{H}_\text{P}$  values is to use water-isotope-  
462 enabled GCMs (Sturm et al., 2010; Conroy et al., 2013; Steen-Larsen et al., 2017). These  
463 estimates of  $\delta^2\text{H}_\text{P}$  values have not typically been used in  $\delta^2\text{H}_{\text{Wax}}$  calibration studies. Because  
464 some of the western Pacific  $\delta^2\text{H}_\text{P}$  values derived from OIPC had such large uncertainties, we  
465 assessed whether scatter in the global relationship between  $\delta^2\text{H}_{\text{Wax}}$  and  $\delta^2\text{H}_\text{P}$  could be reduced by  
466 using isotope-enabled GCMs to estimate  $\delta^2\text{H}_\text{P}$  values (Figure 5).

467 In general,  $\delta^2\text{H}_{\text{Wax}}$  values from *n*-C<sub>28</sub>-acid are better correlated with  $\delta^2\text{H}_\text{P}$  values generated  
468 by isotope-enabled GCMs than  $\delta^2\text{H}_{\text{Wax}}$  values from *n*-C<sub>29</sub>-alkane. This difference may be due to  
469 the distinct spatial distributions of the two calibration data sets, with fatty acid  $\delta^2\text{H}$  values almost  
470 exclusively limited to North America (Figure 1). Sites from which *n*-alkane  $\delta^2\text{H}$  values are  
471 available are more numerous, more globally distributed, and include many measurements from  
472 the Himalayas and Tibetan Plateau (Figure 1). Here, steep elevation gradients may make  $\delta^2\text{H}_\text{P}$   
473 vary on spatial scales that are smaller than the resolution of most models, and fluvial and aeolian  
474 processes may transport waxes between regions with distinct  $\delta^2\text{H}_\text{P}$  values. Overall, our analysis  
475 does not suggest any structural limitations to using the OIPC to estimate  $\delta^2\text{H}_\text{P}$  values for proxy  
476 calibration. However, the limited  $\delta^2\text{H}_\text{P}$  measurements from the tropical Pacific and resulting large  
477 uncertainties in modern estimates from the OIPC or isotope-enabled GCMs remains a  
478 considerable challenge for assessing the fidelity of  $\delta^2\text{H}_{\text{Wax}}$  values in this region.

479 In particular, the orographic effects of mountainous islands may not be adequately captured  
480 by either the OIPC or isotope-enabled GCMs, causing particular challenges determining the  
481 appropriate calibration target for water isotope proxies. For example, the highest peaks on the  
482 island of Espiritu Santo in Vanuatu are nearly 2000 m above sea level. With prevailing winds  
483 from the east, the west coast sits in the rain shadow of the mountains and is significantly drier  
484 than the eastern part of the island (Terry, 2011). However, the only long-term weather station for  
485 the island is located at Pekoa airport in the southeast corner of the island, and there are no local  
486 GNIP stations. Therefore, minimal local data is available to inform precipitation isotope models.  
487 The OIPC predicts equivalent  $\delta^2\text{H}_\text{P}$  values for sites on opposite coasts of Espiritu Santo, and  
488 predicted  $\delta^2\text{H}_\text{P}$  values from water-isotope-enabled GCMs on each coast are within a few ‰ of  
489 each other. However, the leeward western sites should have lighter  $\delta^2\text{H}_\text{P}$  values than the eastern  
490 sites that receive rain from more marine air masses (Scholl et al., 1996, 2007). This expectation

491 is supported by the  $\delta^2\text{H}$  values of lake and stream waters collected during our field campaigns,  
492 which are depleted by 20 – 40 ‰ on the leeward western side of the island compared to the  
493 windward east coast (Data Set S2).

494

#### 495 4.3 Contrasts with $\delta^2\text{H}$ values of non-leaf wax lipids

496 In addition to the longer chain *n*-alkane and *n*-alkanoic acids that are primarily derived  
497 from higher plant waxes, we also measured  $\delta^2\text{H}$  values from several compounds of mixed or  
498 primarily algal sources. These compounds are typically found in sedimentary records along with  
499 leaf waxes, and the different controls on their  $\delta^2\text{H}$  values offer the opportunity to more  
500 completely resolve sources of down-core variability in  $\delta^2\text{H}_{\text{Wax}}$  values. Here we discuss lipids  
501 from algal sources, and ubiquitous compounds produced by most organisms.

502

##### 503 4.3.1 Algal lipids

504 Unlike  $\delta^2\text{H}_{\text{Wax}}$  values,  $\delta^2\text{H}$  values of algal biomarkers are well correlated with tropical  
505 Pacific  $\delta^2\text{H}_{\text{P}}$  values and mean annual precipitation (Figure 2). This is particularly the case for  
506 dinosterol (Maloney et al., 2019), which is primarily produced by dinoflagellates (Volkman,  
507 2003). The  $\delta^2\text{H}$  values of *n*-C<sub>17</sub>-alkane, which is primarily derived from algae (Cranwell et al.,  
508 1987; Meyers, 2003), were also highly correlated with  $\delta^2\text{H}_{\text{P}}$  values (consistent with Sachse et al.,  
509 2004) and inversely correlated with mean annual precipitation (Figure 2). An inverse correlation  
510 between the amount of mean annual precipitation and  $\delta^2\text{H}_{\text{P}}$  values (and therefore  $\delta^2\text{H}$  values of  
511 lipids that track  $\delta^2\text{H}_{\text{P}}$ ) is expected in a low-latitude maritime regions where the amount effect  
512 plays a strong role in determining the isotopic composition of rain (Dansgaard, 1964; Rozanski  
513 et al., 1993; Kurita et al., 2009).

514 One reason why  $\delta^2\text{H}$  values from the algal biomarkers are better correlated with  $\delta^2\text{H}_\text{P}$   
515 values than  $\delta^2\text{H}_\text{Wax}$  values might relate to the source water used by each type of organism. Leaf  
516 waxes from higher plants growing on land may reflect a temporal bias, as monthly OIPC  $\delta^2\text{H}_\text{P}$   
517 values can differ by up to 40‰ at the tropical Pacific sites. Higher plants primarily produce leaf  
518 waxes soon after setting new leaves, meaning that there may be a seasonal bias in the  $\delta^2\text{H}_\text{P}$  signal  
519 that is transferred to their waxes (Tipple et al., 2013; Freimuth et al., 2017). If algae are  
520 productive throughout the year, they may better integrate annual precipitation, therefore resulting  
521 in algal lipids that more closely track mean annual  $\delta^2\text{H}_\text{P}$  values.

522 Another reason why algal biomarkers may track  $\delta^2\text{H}_\text{P}$  better than leaf waxes is that they  
523 come from a more limited range of potential sources. In addition to the range of plant sources for  
524 leaf waxes discussed in section 4.1, many of the mid-chain and relatively long-chained  
525 acetogenic compounds, including *n*-C<sub>29</sub>-alkane and *n*-C<sub>28</sub>-acid, can be derived from a mix of  
526 terrestrial and aquatic plants (Bush & McInerney, 2013; Andrae et al., 2020; Dion-Kirschner et  
527 al., 2020). *n*-C<sub>28</sub>-acid can also be partially derived from microalgal sources (Volkman, 1980; van  
528 Bree et al., 2018). Therefore the leaf waxes may represent variable aquatic and terrestrial  
529 contributions, while the algal compounds are always aquatically sourced.

530 Finally, the spatial variability integrated by each type of compound could explain the  
531 different trends in their  $\delta^2\text{H}_\text{Wax}$  values. Algal lipids are produced within the relatively confined  
532 space of the lake or pond overlaying the sediments in which they accumulate. Leaf waxes can be  
533 derived from plants growing adjacent to their depositor, but also from further afield in the  
534 catchment, and the relative size of the catchment area can differ among water bodies.  
535 Additionally, > 20% of leaf waxes accumulating in sediment can come from aerosols, which can  
536 be transported long distances and have  $\delta^2\text{H}$  values distinct from local vegetation (Conte et al.,  
537 2003; Gao et al., 2014; Nelson et al., 2017; Nelson et al., 2018). Leaf wax aerosols from very

538 distant sites may have more impact on lake sediments on islands than on continents, since there  
539 is a relatively smaller contiguous land area to contribute regional and local waxes. On the other  
540 hand, the overall contribution of local leaf waxes may be significantly higher on small islands  
541 where all non-local leaf waxes must be carried great distances.

542

#### 543 4.3.2 Generic fatty acids

544 In contrast to the algal specific biomarkers dinosterol and *n*-C<sub>17</sub>-alkane,  $\delta^2\text{H}$  values of *n*-  
545 C<sub>16</sub> and *n*-C<sub>18</sub> fatty acids were positively correlated with mean annual precipitation and  
546 negatively correlated with  $\delta^2\text{H}_\text{P}$  (Figure 2). These shorter chain fatty acids are synthesized by  
547 most organisms, but are frequently attributed to algal sources in aquatic sediments (Huang et al.,  
548 2004; Li et al. 2009). Heterotrophic and chemoautotrophic microbes produce short-chain fatty  
549 acids that can have  $\delta^2\text{H}$  values that differ by several hundred ‰ from those of photoautotrophs  
550 grown in similar water (Zhang et al., 2009; Heinzemann et al., 2015). However, other than in  
551 microbial mats (Osburn et al., 2011), sedimentary *n*-C<sub>16</sub> and *n*-C<sub>18</sub> fatty acids typically have  
552 fractionation factors consistent with values from photoautotrophs in culture (Li et al, 2009;  
553 Zhang et al., 2009; Heinzemann et al., 2018). In our tropical Pacific data set, fractionation  
554 factors between lake water and *n*-C<sub>16</sub> and *n*-C<sub>18</sub>-acids ( $\alpha_{\text{Lipid-Water}} = (^2\text{H}/^1\text{H})_{\text{Lipid}} / (^2\text{H}/^1\text{H})_{\text{Water}}$ )  
555 ranged from 0.773 to 0.920. This large range in  $\alpha_{\text{Lipid-Water}}$  values is consistent with observations  
556 of cultures of different types of algae (Zhang and Sachs, 2007; Zhang et al., 2009; Heinzemann  
557 et al., 2015). The  $\delta^2\text{H}$  values of the *n*-C<sub>16</sub> and *n*-C<sub>18</sub>-acids in our data set could be influenced by  
558 variable contributions from non-photoautotrophs, but could also vary due to differing  
559 contributions from different types of algae. In either case, it seems likely that  $\delta^2\text{H}$  values of these  
560 compounds reflect ecology more than hydroclimate, and their negative correlations with  $\delta^2\text{H}_\text{P}$   
561 values in our sample set may be a coincidence. Dinosterol and *n*-C<sub>17</sub>-alkane are sourced from a

562 smaller range of organisms than the near ubiquitous  $n\text{-C}_{16}$  and  $n\text{-C}_{18}$ -acids (Cranwell et al., 1987;  
563 Meyers, 2003; Volkman, 2003), which could make their  $\delta^2\text{H}$  values more directly related to  
564 those of lake water.

565

#### 566 4.4 Implications for paleoclimate reconstructions in the tropical Pacific

567 Although  $\delta^2\text{H}_{\text{Wax}}$  values are strongly linearly correlated with  $\delta^2\text{H}_{\text{P}}$  values on a global scale  
568 (Figure 3), the large residuals in this relationship indicate that caution should be applied before  
569 interpreting relatively small down-core changes in  $\delta^2\text{H}_{\text{Wax}}$  values as hydroclimate changes.  
570 However, our data do not suggest that there are clear links between vegetation source (as  
571 indicated by palynological analyses) and residuals from the global  $\delta^2\text{H}_{\text{Wax}}\text{-}\delta^2\text{H}_{\text{P}}$  relationship  
572 (Figure 6). Rather, one of the largest challenges for interpreting sedimentary  $\delta^2\text{H}_{\text{Wax}}$  values in the  
573 tropical Pacific are uncertainties associated with modern estimates of  $\delta^2\text{H}_{\text{P}}$  values, given the  
574 limited spatial and temporal available of modern observations. Recent isotope modeling work  
575 has helped constrain the processes that control  $\delta^2\text{H}_{\text{P}}$  values in this dynamically important region  
576 (Conroy et al., 2016; Konecky et al., 2019). Continued effort in this regard is necessary to  
577 robustly interpret proxies  $\delta^2\text{H}_{\text{P}}$  values, whether they are derived from  $\delta^2\text{H}_{\text{Wax}}$  values or from  
578 other archives such as speleothems.

579 The expected inverse correlation between precipitation amount and OIPC-derived  $\delta^2\text{H}_{\text{P}}$   
580 values in the tropical Pacific, and the correlations between these variables and algal lipid  $\delta^2\text{H}$   
581 values (Maloney et al., 2019), suggest that the uncertainty in  $\delta^2\text{H}_{\text{P}}$  values cannot be solely  
582 responsible for the poor correlations associated with  $\delta^2\text{H}_{\text{Wax}}$  values (Figure 2). Rather, factors  
583 besides  $\delta^2\text{H}_{\text{P}}$  values that influence  $\delta^2\text{H}_{\text{Wax}}$  values (variations in seasonality, catchment scales,  
584 contributions from organs other than leaves and/or from aquatic sources, or changes in  
585 biosynthetic fractionation) result in residuals that are on the order of  $\pm 25\%$  in the tropical Pacific

586 and elsewhere (Figure 3). Any calibration of  $\delta^2\text{H}_{\text{Wax}}$  values spanning a relatively small range of  
587  $\delta^2\text{H}_{\text{P}}$  values (like the 32‰ range studied here) is likely to have a poor correlation between the  
588 two variables (Figure 4). Correlation coefficients for the tropical Pacific are within the  
589 distribution generated by randomly subsampling the global data set while limiting the range in  
590  $\delta^2\text{H}_{\text{P}}$  to 35‰, but fall towards the low end of this range, more than 1 standard deviation below  
591 the mean correlation coefficient (Figure 4).

592 Regional calibrations are expected to have stronger than average correlations by  
593 constraining some variables that contribute to scatter in the global relationship between  $\delta^2\text{H}_{\text{P}}$  and  
594  $\delta^2\text{H}_{\text{Wax}}$  values. However, the new data from the tropical Pacific exceed a regional scale in many  
595 ways, spanning a distance of ~8500 km, larger than even continental-scale studies (e.g., Sachse  
596 et al., 2004). The islands included range from low-lying atolls to mountainous volcanoes. The  
597 sites differ in seasonality of precipitation, vulnerability to tropical storms, sensitivity to El  
598 Niño–Southern Oscillation events, and biodiversity, all of which may impact  $\delta^2\text{H}_{\text{Wax}}$  values. The  
599 diversity of sites, uncertainty in local estimates of  $\delta^2\text{H}_{\text{P}}$  values, and small  $\delta^2\text{H}_{\text{P}}$  signal relative to  
600 the noise in the global calibration, make it unsurprising that  $\delta^2\text{H}_{\text{Wax}}$  values are not correlated with  
601  $\delta^2\text{H}_{\text{P}}$  values within the tropical Pacific. However, it is encouraging that tropical Pacific  $\delta^2\text{H}_{\text{Wax}}$   
602 values fall within the expected range, and do not have abnormally large residuals from the global  
603 calibration line. Together, these results suggest that the processes determining  $\delta^2\text{H}_{\text{Wax}}$  values in  
604 tropical Pacific lake and swamp sediments are not fundamentally different than elsewhere.

605 The scatter in the global relationship between  $\delta^2\text{H}_{\text{P}}$  and  $\delta^2\text{H}_{\text{Wax}}$  (Figure 3) suggests that  
606 down-core changes as large as ~50‰ at any location could be driven by factors other than  $\delta^2\text{H}_{\text{P}}$   
607 values. In practice, at a single site where many variables that contribute to scatter among sites are  
608 constant, the threshold for detecting changes in  $\delta^2\text{H}_{\text{P}}$  values may be significantly smaller.

609 Detailed processed-based studies at the catchment scale (Freimuth et al., 2019, 2020; Dion-

610 Kirschner et al., 2020) may be more useful for constraining sedimentary  $\delta^2\text{H}_{\text{Wax}}$  than additional  
 611 large-scale calibration efforts.

612 Hydroclimate-driven interpretations of changes in sedimentary  $\delta^2\text{H}_{\text{Wax}}$  values will be  
 613 most robust when supported by independent lines of proxy evidence, such as  $\delta^2\text{H}$  values of more  
 614 source specific biomarkers like dinosterol (Smittenberg et al., 2011; Nelson & Sachs, 2016;  
 615 Richey & Sachs, 2016; Sachs et al., 2018), changes in grain size distributions (Conroy et al.,  
 616 2008), or changes in the elemental composition of inorganic sediments (Sear et al 2020; Higley  
 617 et al., 2018). Continued refinement of a multi-proxy toolbox that includes sedimentary  $\delta^2\text{H}_{\text{Wax}}$   
 618 values offers the best path to confidently reconstructing past hydrologic change.

## 619 **5 Conclusions**

620  $\delta^2\text{H}_{\text{Wax}}$  values from surface sediments from 19 lakes and four swamps on 15 islands  
 621 throughout the tropical Pacific fall within the overall range of values expected based on a global  
 622 compilation surface sediment measurements ( $R^2 = 0.74$  for both  $n\text{-C}_{29}$ -alkane ( $n = 665$ ) and  $n\text{-}$   
 623  $\text{C}_{28}$ -acid ( $n = 242$ )), and the residuals around the global linear regression between  $\delta^2\text{H}_{\text{Wax}}$  and  
 624  $\delta^2\text{H}_{\text{P}}$  are similar in the tropical Pacific and global data sets. Nevertheless, within the tropical  
 625 Pacific there is no significant correlation between  $\delta^2\text{H}_{\text{Wax}}$  and  $\delta^2\text{H}_{\text{P}}$  values. The lack of correlation  
 626 regionally is at least partly due to the large uncertainties in  $\delta^2\text{H}_{\text{P}}$  values derived from reanalysis  
 627 data and cannot be ascribed to different vegetation sources within and surrounding the lakes in  
 628 this study, as deduced from pollen assemblages.

629 To a first order on a global scale,  $\delta^2\text{H}_{\text{Wax}}$  values are clearly influenced by  $\delta^2\text{H}_{\text{P}}$  values, but  
 630 the  $\delta^2\text{H}_{\text{P}}$  signal spanning the tropical Pacific remains small relative to the noise in the current  
 631 global calibration. The global  $\delta^2\text{H}_{\text{Wax-P}}$  calibration remains limited by uncertainties in both the x-  
 632 and y-axes, and could be improved by better constraints on  $\delta^2\text{H}_{\text{P}}$  values. As in other locations,

633 large changes in  $\delta^2\text{H}_{\text{Wax}}$  in sediments from tropical Pacific islands may be caused by variables  
634 other than  $\delta^2\text{H}_\text{P}$ , and could be improved by more catchment-scale, processed-based studies. In  
635 particular, interpretations need to consider the possible effects of changing source, growth  
636 conditions, and delivery of leaf waxes to sediments. When possible,  $\delta^2\text{H}_{\text{Wax}}$  values should be  
637 paired with  $\delta^2\text{H}$  values of more source-specific compounds such as dinosterol, which can help  
638 distinguish changes in water isotopes from changes in other factors that affect  $\alpha_{\text{Wax-P}}$  values. As  
639 is the case for all paleoclimate proxies, interpretations of  $\delta^2\text{H}_{\text{Wax}}$  values are most robust in a  
640 multiproxy context.

#### 641 **Acknowledgments, Samples, and Data**

642 Funding was provided by a Swiss National Science Foundation grant to ND (Grant Nr.  
643 PP00P2\_163782), a National Science Foundation grant to JPS (Grant No. 1502417), a NERC  
644 grant to DAS (NE/N00674/1), and an Australian Research Council grant to MP (DP0985593).  
645 Carsten Schubert hosted NL for laboratory work and provided necessary instrumentation.  
646 Nichola Strandberg provided pollen data from Lake Hut. Christiane Krentscher helped with  
647 sample processing in addition to those acknowledged by Maloney et al. (2019). Julie Richey and  
648 many others helped with sample collection, as acknowledged by Maloney et al. (2019) and  
649 Krentscher et al. (2019). All data associated with this manuscript is freely available in the ETH  
650 data repository (doi: 10.3929/ethz-b-000412154).

#### 651 **Figure captions**

652 **Figure 1** Global distribution of leaf wax samples from surface sediments and soils. The left  
653 panel shows the locations for  $n\text{-C}_{29}$ -alkane (665 sites); the right panel shows the locations for  $n\text{-}$   
654  $\text{C}_{28}$ -acid (242 sites). Background shading represents annual mean  $\delta^2\text{H}_\text{P}$  values from the Online  
655 Isotopes in Precipitation Calculator (OIPC) (Bowen & Ravenaugh, 2003; IAEA/WMO, 2015;  
656 Bowen, 2020). OIPC does not produce spatial data sets over marine areas, therefore shading is  
657 limited to continents.

658  
659 **Figure 2:** Correlation coefficients of linear regressions of  $\delta^2\text{H}$  values of all analyzed compounds  
660 relative to  $\delta^2\text{H}_\text{P}$  values (blue circles) and mean annual precipitation (pink diamonds) in the  
661 tropical Pacific. Filled symbols represent significant correlations at the 95% confidence level.  
662 Mean annual precipitation is from the Global Precipitation Climatology Project (GPCP) and  $\delta^2\text{H}_\text{P}$   
663 values are from the OIPC. Compounds are grouped by source (algal, general, or plant waxes,  
664 with increasingly likely terrestrial plant sources associated with longer chain lengths). Dinosterol  
665  $\delta^2\text{H}$  data is from Maloney et al. (2019), all other lipid  $\delta^2\text{H}$  data from this study. Individual  
666 measurements are included in Data Set S1.

667

668 **Figure 3**  $\delta^2\text{H}$  values of (a, c)  $n\text{-C}_{29}$ -alkane and (b, d)  $n\text{-C}_{28}$ -acid from surface sediments and soils  
 669 plotted relative to OIPC-derived  $\delta^2\text{H}_\text{P}$  values, color-coded by region (a, b), and sample type (c,  
 670 d). In panels a and b, red diamonds are lakes from the SPCZ region and green squares are  
 671 mangrove swamps in Micronesia (this study), both plotted with error bars. X-axis error bars  
 672 represent 95% confidence intervals of OIPC values. Y-axis error bars represent 1 standard  
 673 deviation of measurements from replicate samples from the same lake or swamp and are  
 674 typically smaller than the marker size. Circles are global values compiled from the literature,  
 675 color-coded by region. X-axis error bars are not shown for previously published data points, and  
 676 average 5.2‰ for sites outside the tropical Pacific. Regression statistics in (a) and (b) are shown  
 677 with and without new Pacific data. Globally compiled data (including tropical Pacific values) do  
 678 not differ significantly between soils and lacustrine sediments for either (c)  $n\text{-C}_{29}$ -alkane or (d)  $n\text{-C}_{28}$ -  
 679  $\text{C}_{28}$ -acid. Shading around linear regressions represents 95% confidence intervals.

680  
 681 **Figure 4** Correlation coefficients of random subsamples of 17 values from the global  
 682 compilation surface sediment and soil of (a)  $n\text{-C}_{29}$ -alkane and (b)  $n\text{-C}_{28}$ -acid  $\delta^2\text{H}$  values plotted  
 683 relative to range of  $\delta^2\text{H}_\text{P}$  values. Subsampled data were taken from the full data set and from  
 684 restricted  $\delta^2\text{H}_\text{P}$  ranges as described in the text. Correlation coefficients for the global compilation  
 685 and each continent are plotted for comparison.

686  
 687 **Figure 5** Correlation plots of  $\delta^2\text{H}$  values from the global compilation of surface sediments and  
 688 soils relative to the  $\delta^2\text{H}_\text{P}$  values from various models (described in section 2.4). Numbers, colors,  
 689 and the widths of the ellipses correspond to correlation coefficients (R values).

690  
 691 **Figure 6** Pollen distributions from surface or near surface sediments in tropical Pacific lake  
 692 samples plotted relative to residuals from the global  $\delta^2\text{H}_{\text{Wax}} - \delta^2\text{H}_\text{P}$  calibration line for (a)  $n\text{-C}_{29}$ -  
 693 alkane and (b)  $n\text{-C}_{28}$ -acid. Square and triangle symbols are used to distinguish among multiple  
 694 sites with the same residual values.

695

## 696 References

- 697 Adler R. F., Huffman, G. J., Chang, A., Ferraro, R., Xie, P.-P., Janowiak, J., et al. (2003). the  
 698 version-2 Global Precipitation in Climatology Project (GPCP) monthly precipitation  
 699 analysis (1979 -- Present). *Journal of Hydrometeorology*, 4(6), 1147-1167.
- 700 Aichner, B., Herzsuh, U., Wilkes, H., Vieth, A., Böhner, & J. (2010).  $\delta\text{D}$  values of n-alkanes  
 701 in Tibetan lake sediments and aquatic macrophytes—A surface sediment study and  
 702 application to a 16 ka record from Lake Koucha. *Organic Geochemistry*, 41(8), 779-790.  
 703 <https://doi.org/10.1016/j.orggeochem.2010.05.010>
- 704 Aichner, B., Hilt, S., Périllon, C., Gillefalk, M., & Sachse, D. (2017). Biosynthetic hydrogen  
 705 isotopic fractionation factors during lipid synthesis in submerged aquatic macrophytes:  
 706 Effect of groundwater discharge and salinity. *Organic Geochemistry*, 113, 10-16.  
 707 <https://doi.org/10.1016/j.orggeochem.2017.07.021>
- 708 Alongi D. M. (2014). Carbon cycling and storage in mangrove forests. *Annual Review of Marine*  
 709 *Science*, 6, 195-219. <https://doi.org/10.1146/annurev-marine-010213-135020>

- 710 Andrae, J. W., McInerney, F. A., & Kale Sniderman, J. M. (2020). Carbon isotope systematics of  
 711 leaf wax *n*-alkanes in a temperate lacustrine depositional environment. *Organic*  
 712 *Geochemistry*, 150, 104121. <https://doi.org/10.1016/j.orggeochem.2020.104121>
- 713 Bai, Y., Fang, X., Gleixner, G., & Mügler, I. (2011). Effect of precipitation regime on dD  
 714 valuesügler, I., 2011. Effect of precipitation regime on  $\delta$ D values of soil *n*-alkanes from  
 715 elevation gradients – implications for the study of paleoelevation. *Organic Geochemistry*,  
 716 42(7), 838-845. <https://doi.org/10.1016/j.orggeochem.2011.03.019>
- 717 Bakkelund, A., Porter, T. J., Froese, D. G., & Feakins, S. J. (2018). Net fractionation of  
 718 hydrogen isotopes in *n*-alkanoic acids from soils in the northern boreal forest. *Organic*  
 719 *Geochemistry*, 125, 1-13. <https://doi.org/10.1016/j.orggeochem.2018.08.005>
- 720 Bowen, G. J. (2020). The Online Isotopes in Precipitation Calculator, version 3.1.  
 721 <http://www.waterisotopes.org>.
- 722 Bowen, G. J., & Ravenaugh, J. (2003). Interpolating the isotopic composition of modern  
 723 meteoric precipitation. *Water Resources Research*, 39(10), 1-13.  
 724 <https://doi.org/10.1029/2003WR002086>
- 725 Bowen, G. J., Cai, Z., Fiorella, R. P., & Putman, A. L. (2019). Isotopes in the water cycle:  
 726 regional- to global-scale patterns and applications. *Annual Review of Earth and Planetary*  
 727 *Sciences*, 47, 453-479. <https://doi.org/10.1146/annurev-erath-053018-060220>
- 728 Brinkmann, N., Seeger, S., Weiler, M., Buchmann, N., Eugster, W., & Kahmen, A. (2018).  
 729 Employing stable isotopes to determine the residence times of soil water and the temporal  
 730 origin of water taken up by *Fagus sylvatica* and *Picea abies* in a temperate forest. *New*  
 731 *Phytologist*, 219(4), 1300-1313. <https://doi.org/10.1111/nph.15255>
- 732 Brown, J. R., Moise, A. F., & Delage, F. P. (2011). Changes in the South Pacific Convergence  
 733 Zone in IPCC AR4 future climate projections. *Climate Dynamics*, 39, 1-19. <https://doi.org/10.1007/s00382-011-1192-0>
- 734 Bush, R. T., & Mcinerney, F. A. (2013). Leaf wax *n*-alkane distributions in and across modern  
 735 plants: implications for paleoecology and chemotaxonomy. *Geochimica et Cosmochimica*  
 736 *Acta*, 117, 161-179. <https://doi.org/10.1016/j.gca.2013.04.016>
- 737 Calvo, E., Marshall, J. F., Pelejero, C., McCulloch, M. T., Gagan, M. K., & Lough, J. M. (2007).  
 738 Interdecadal climate variability in the Coral Sea since 1708 A.D. *Palaeogeography*,  
 739 *Palaeoclimatology, Palaeoecology*, 248(1-2), 190-201.  
 740 <https://doi.org/10.1016/j.palaeo.2006.12.003>
- 741 Cernusak, L. A., Barbour, M. M., Arndt, S. K., Cheesman, A. W., English, N. B., Feild, T. S., et  
 742 al. (2016). Stable isotopes in leaf water of terrestrial plants. *Plant, Cell and Environment*,  
 743 39(5), 1087-1102. <https://doi.org/10.1111/pce.12703>
- 744 Chikaraishi Y., & Naraoka H. (2003). Compound-specific  $\delta$ D- $\delta^{13}$ C analyses of *n*-alkanes  
 745 extracted from terrestrial and aquatic plants. *Phytochemistry*, 63(3), 361–371.  
 746 [https://doi.org/10.1016/S0031-9422\(02\)00749-5](https://doi.org/10.1016/S0031-9422(02)00749-5)
- 747 Conroy, J. L., Cobb, K. M., & Noone, D. (2013). Comparison of precipitation isotope variability  
 748 across the tropical Pacific in observations and SWING2 model simulations. *JGR*  
 749 *Atmospheres*, 118(11), 5867-5829. <https://doi.org/10.1002/jgrd.50412>
- 750 Conroy, J. L., Noone, D., Cobb, K. M., Moerman, J. W., & Konecky, B. L. (2016). Paired stable  
 751 isotopologues in precipitation and vapor: A case study of the amount effect within western  
 752 tropical Pacific storms. *JGR Atmospheres*, 121(7), 3290-3303.  
 753 <https://doi.org/10.1002/2015JD023844>
- 754

- 755 Conte, M. H., Weber, J. C., Carlson, P. J., & Flanagan, L. B. (2003). Molecular and carbon  
756 isotopic composition of leaf wax in vegetation and aerosols in a northern prairie  
757 ecosystem. *Oecologia*, 135, 67-77. <https://doi.org/10.1007/s00442-002-1157-4>
- 758 Cormier, M. -A., Werner, R. A., Sauer, P. E., Grocke, D. R., Leuenberger, M. C., Wieloch, T., et  
759 al. (2018).  $^2\text{H}$ -fractionations during the biosynthesis of carbohydrates and lipids imprint a  
760 metabolic signal on the  $\delta^2\text{H}$  values of plant organic compounds. *New Phytologist*, 218(2),  
761 479-491. <https://doi.org/10.1111/nph.15016>
- 762 Cranwell, P. A., Eglinton, G., & Robinson, N. (1987). Lipid of aquatic organisms as potential  
763 contributors to lacustrine sediments II. *Organic Geochemistry*, 11(6), 513-527.  
764 [https://doi.org/10.1016/0146-6380\(87\)90007-6](https://doi.org/10.1016/0146-6380(87)90007-6)
- 765 Daniels, W. C., Russell, J. M., Giblin, A. E., Welker, J. M., Klein, E. S., & Huang, Y. (2017).  
766 Hydrogen isotope fractionation in leaf waxes in the Alaskan Arctic tundra. *Geochimica et*  
767 *Cosmochimica Acta*, 213, 216-236. <https://doi.org/10.1016/j.gca.2017.06.028>
- 768 Dansgaard, W. (1964). Stable isotopes in precipitation. *Tellus*, 16, 436-469.  
769 <https://doi.org/10.1111/j.2153-3490.1964.tb00181.x>
- 770 DeLong, K. L., Quinn, T. M., Taylor, F. W., Lin, K., & Shen, C. -C. (2012). Sea surface  
771 temperature variability in the southwest tropical Pacific since 1649. *Nature Climate*  
772 *Change*, 2, 799-804. <https://doi.org/10.1038/NCLIMATE1583>
- 773 Dion-Kirschner, H., McFarlin, J. M., Masterson, A. L., Axford, Y., & Osburn, M. R. (2020).  
774 Modern constraints on the sources and climate signals recorded by sedimentary plant  
775 waxes in west Greenland. *Geochimica et Cosmochimica Acta*, 286, 336-354.  
776 <https://doi.org/10.1016/j.gca.2020.07.027>
- 777 Douglas, P. M. J., Pagani, M., Brenner, M., Hodell, D. A., & Curtis, J. H. (2012). Aridity and  
778 vegetation composition are important determinants of leaf-wax  $\delta\text{D}$  values in southeastern  
779 Mexico and Central America. *Geochimica et Cosmochimica Acta*, 97, 24-45.  
780 <https://doi.org/10.1016/j.gca.2012.09.005>
- 781 Eley, Y., Dawson, L., Black, S., Andrews, J., & Pendentchouk, N. (2014). Understanding  $^2\text{H}/^1\text{H}$   
782 systematics of leaf wax *n*-alkanes in coastal plants at Stiffkey saltmarsh, Norfolk, UK.  
783 *Geochimica et Cosmochimica Acta*, 128, 13-28. <https://doi.org/10.1016/j.gca.2013.11.045>
- 784 Feakins, S. J., & Sessions, A. L. (2010). Controls on the D/H ratios of plant leaf waxes in an arid  
785 ecosystem. *Geochimica et Cosmochimica Acta*, 74(7), 2128-2141.  
786 <https://doi.org/10.1016/j.gca.2010.01.016>
- 787 Feng, X., D'Andrea, W. J., Zhao, C., Xin, S., Zhang, C., & Liu, W. (2019). Evaluation of leaf  
788 wax  $\delta\text{D}$  and soil brGDGTs as tools for paleoaltimetry on the southeastern Tibetan Plateau.  
789 *Chemical Geology*, 523, 95-106. <https://doi.org/10.1016/j.chemgeo.2019.05.005>
- 790 Ficken, K. J., Li, B., Swain, D. L., & Eglinton, G. (2000). An *n*-alkane proxy for the sedimentary  
791 input of submerged/floating freshwater aquatic macrophytes. *Organic Geochemistry*, 31(7-  
792 8), 745-749. [https://doi.org/10.1016/S0146-6380\(00\)00081-4](https://doi.org/10.1016/S0146-6380(00)00081-4)
- 793 Freimuth, E. J., Diefendorf, A. F., & Lowell, T. V. (2017). Hydrogen isotopes of *n*-alkanes and  
794 *n*-alkanoic acids as tracers of precipitation in a temperate forest and implications for  
795 paleorecords. *Geochimica et Cosmochimica Acta*, 206, 166-183.  
796 <https://doi.org/10.1016/j.gca.2017.02.027>
- 797 Freimuth, E. J., Diefendorf, A. F., Lowell, T. V., Bates, B. R., Schartman, A., Bird, B. W., et al.  
798 (2020). Contrasting sensitivity of lake sediment *n*-alkanoic acids and *n*-alkanes to basin-  
799 scale vegetation and regional-scale precipitation  $\delta^2\text{H}$  in the Adirondack Mountains, NY  
800 (USA). *Geochimica et Cosmochimica Acta*, 268, 22-41.  
801 <https://doi.org/10.1016/j.gca.2019.08.026>

- 802 Freimuth, E. J., Diefendorf, A. F., Lowell, T. V., & Wiles, G. C. (2019). Sedimentary n-alkanes  
803 and n-alkanoic acids in a temperate bog are biased toward woody plants. *Organic*  
804 *Geochemistry*, 128, 94-107 <https://doi.org/10.1016/j.orggeochem.2019.01.006>
- 805 Gamarra, B., & Kahmen, A. (2015). Concentrations and  $\delta^2\text{H}$  values of cuticular n-alkanes vary  
806 significantly among plant organs, species and habitats in grasses from an alpine and a  
807 temperate European grassland. *Oecologia*, 178, 981-998. [https://doi.org/10.1007/s00442-](https://doi.org/10.1007/s00442-015-3278-6)  
808 015-3278-6
- 809 Gao L., Edwards E. J., Zeng Y., & Huang Y. (2014). Major Evolutionary Trends in Hydrogen  
810 Isotope Fractionation of Vascular Plant Leaf Waxes. *PLoS ONE*, 9(11): e112610.  
811 <https://doi.org/10.1371/journal.pone.0112610>
- 812 Gao, L., Hou, J., Toney, J., MacDonald, D., & Huang, Y. (2011). Mathematical modeling of the  
813 aquatic macrophyte inputs of mid-chain n-alkyl lipids to lake sediments: implications for  
814 interpreting compound specific hydrogen isotopic records. *Geochimica et Cosmochimica*  
815 *Acta*, 75(13), 3781-3791. <https://doi.org/10.1016/j.gca.2011.04.008>
- 816 Garcin, Y., Schwab, V. F., Gleixner, G., Kahmen, A., Todou, G., Sene, O., et al. (2012).  
817 Hydrogen isotope ratios of lacustrine sedimentary n-alkanes as proxies of tropical African  
818 hydrology: insights from a calibration transect across Cameroon. *Geochimica et*  
819 *Cosmochimica Acta*, 79, 106-126. <https://doi.org/10.1016/j.gca.2011.11.039>
- 820 Gillespie, T. W., Keppel, G., Pau, S., Price, J. P., Jaffre, T., & O'Neill, K. (2013). Scaling  
821 species richness and endemism of tropical dry forests on oceanic islands. *Diversity and*  
822 *Distributions*, 19(8), 896-906. <https://doi.org/10.1111/ddi.12036>
- 823 Goldsmith, Y., Polissar, P. J., deMenocal, P. B., & Broecker, W. S. (2019). Leaf wax  $\delta\text{D}$  and  
824  $\delta^{13}\text{C}$  in soils record hydrological and environmental information across a climatic gradient  
825 in Israel. *Journal of Geophysical Research: Biogeosciences*, 124, 2898-2916.  
826 <https://doi.org/10.1029/2019JG005149>
- 827 Gosling, W. D., Sear, D. A., Hassall, J. D., Langdon, P. G., Bönner, M. N. T., Driessen, T. D., &  
828 McMichael, C. N. H. (2020). Human occupation and ecosystem change on Upolu (Samoa)  
829 during the Holocene. *Journal of Biogeography*, 47(3), 600-  
830 614. <https://doi.org/10.1111/jbi.13783>
- 831 Hassall, J. D. (2017). Static or dynamic: Reconstructing past movement of the South Pacific  
832 Convergence Zone. University of Southampton.
- 833 He, D., Ladd, S. N., Sachs, J. P., & Jaffé, R. (2017). Inverse relationship between salinity and  
834  $^2\text{H}/^1\text{H}$  fractionation in leaf wax n-alkanes from Florida mangroves. *Organic Geochemistry*,  
835 110, 1-12. <https://doi.org/10.1016/j.orggeochem.2017.04.007>
- 836 He, D., Ladd, S. N., Saunders, C. J., Mead, R. N., & Jaffé, R. (2020). Distribution of n-alkanes  
837 and their  $\delta^2\text{H}$  and  $\delta^{13}\text{C}$  values in typical plants along a terrestrial-coastal-oceanic gradient.  
838 *Geochimica et Cosmochimica Acta*, 281, 31-52. <https://doi.org/10.1016/j.gca.2020.05.003>
- 839 Hendy, E. J., Gagan, M. K., Alibert, C. A., McCulloch, M. T., Lough, J. M., & Isdale, P. J.  
840 (2002). Abrupt decrease in tropical Pacific sea surface salinity at end of Little Ice Age.  
841 *Science*, 295(5559), 1511-1514. <https://doi.org/10.1126/science.1067693>
- 842 Heinzemann, S. M., Villanueva, L., Lipsewiers, Y. A., Sinke-Schoen, D., Sinninghe Damsté, J.  
843 S., Schouten, S., & van der Meer, M. T. J. (2018). Assessing the metabolism of  
844 sedimentary microbial communities using the hydrogen isotope composition of fatty acids.  
845 *Organic Geochemistry*, 124, 123-132. <https://doi.org/10.1016/j.orggeochem.2018.07.011>
- 846 Heinzemann S. M., Villanueva L., Sinke-Schoen D., Sinninghe Damsté J. S., Schouten S., &  
847 van der Meer M. T. J. (2015). Impact of metabolism and growth phase on the hydrogen

- 848 isotopic composition of microbial fatty acids. *Frontiers in Microbiology*, 6, 408.  
849 <https://doi.org/10.3389/fmicb.2015.00408>
- 850 Higley, M. C., Conroy, J. L., & Schmitt, S. (2018). Last Millennium Meridional Shifts in  
851 Hydroclimate in the Central Tropical Pacific. *Paleoceanography and Paleoclimatology*,  
852 33(4), 354-366. <https://doi.org/10.1002/2017PA003233>
- 853 Hope, G. S., & Pask, J. (1998). Tropical vegetational change in the late Pleistocene of New  
854 Caledonia. *Palaeogeography, Palaeoclimatology, Palaeoecology*, 142(1-2), 1-21.  
855 [https://doi.org/10.1016/S0031-0182\(97\)00140-5](https://doi.org/10.1016/S0031-0182(97)00140-5)
- 856 Hou, J., D'Andrea, W., & Huang, Y. (2008). Can sedimentary leaf waxes record D/H ratios of  
857 continental precipitation? Field, model and experimental assessments. *Geochimica et*  
858 *Cosmochimica Acta*, 72(14), 3503-3517. <https://doi.org/10.1016/j.gca.2008.04.030>
- 859 Huang, Y., Shuman, B., Wang, Y., & Webb III, T. (2004). Hydrogen isotope ratios of individual  
860 lipids in lake sediments as novel tracers of climatic and environmental change: a surface  
861 sediment test. *Journal of Paleolimnology*, 31, 363-375.  
862 <https://doi.org/10.1023/B:JOPL.0000021855.80535.13>
- 863 IAEA/WMO (2015). Global Network of Isotopes in Precipitation. The GNIP Database.  
864 Accessible at: <https://nucleus.iaea.org/wiser>.
- 865 Jia, G., Wei, K., Chen, F., & Peng, P. (2008). Soil *n*-alkane  $\delta$ D vs. altitude gradients along  
866 Moug Gongga, China. *Geochimica et Cosmochimica Acta*, 72(21), 5165-5174.  
867 <https://doi.org/10.1016/j.gca.2008.08.004>
- 868 Kahmen, A., Hoffmann, B., Schefuss, E., Arndt, S. K., Cernusak, L. A., West, J. B., & Sachse,  
869 D. (2013). Leaf water deuterium enrichment shapes leaf wax *n*-alkane  $\delta$ D values of  
870 angiosperm plants II: Observational evidence and global implications. *Geochimica et*  
871 *Cosmochimica Acta*, 111, 50–63. <https://doi.org/10.1016/j.gca.2012.09.004>
- 872 Konecky, B. L., Noone, D. C., & Cobb, K. M. (2019). The influence of competing hydroclimate  
873 processes on stable isotope ratios in tropical rainfall. *Geophysical Research Letters* 46(3),  
874 1622-1633. <https://doi.org/10.1029/2018GL080188>
- 875 Konecky, B. L., Russell, J., & Bijaksana, S. (2016). Glacial aridity in central Indonesia coeval  
876 with intensified monsoon circulation. *Earth and Planetary Science Letters* 437, 15-24.  
877 <https://doi.org/10.1016/j.epsl.2015.12.037>
- 878 Krentscher, C., Dubois, N., Camperio, G., Prebble, M., Ladd, S.N., 2019. Palmitone as a  
879 potential species-specific biomarker for the crop plant taro (*Colocasia esculenta Schott*) on  
880 remote Pacific islands. *Organic Geochemistry*, 132, 1-10.  
881 <https://doi.org/10.1016/j.orggeochem.2019.03.006>
- 882 Kurita, N., Ichiyanagi, K., Matsumoto, J., Yamanaka, M. D., & Ohata, T. (2009). The  
883 relationship between the isotopic content of precipitation and the precipitation amount in  
884 tropical regions. *Journal of Geochemical Exploration*, 102(3), 113-122.  
885 <https://doi.org/10.1016/j.gexplo.2009.03.002>
- 886 Ladd S. N., & Sachs J. P. (2012). Inverse relationship between salinity and *n*-alkane  $\delta$ D values in  
887 the mangrove *Avicennia marina*. *Organic Geochemistry*, 48, 25–36.  
888 <https://doi.org/10.1016/j.orggeochem.2012.04.009>
- 889 Ladd, S. N., & Sachs, J. P. (2015). Influence of salinity on hydrogen isotope fractionation in  
890 *Rhizophora* mangroves from Micronesia. *Geochimica et Cosmochimica Acta*, 168, 206–  
891 221. <https://doi.org/10.1016/j.gca.2015.07.004>
- 892 Ladd, S. N., & Sachs, J. P. (2017).  $^2\text{H}/^1\text{H}$  fractionation in lipids of the mangrove *Bruguiera*  
893 *gymnorhiza* increases with salinity in marine lakes of Palau. *Geochimica et Cosmochimica*  
894 *Acta*, 204, 300-312. <https://doi.org/10.1016/j.gca.2017.01.046>

- 895 Ladd, S. N., Nelson, D. B., Schubert, C. J., & Dubois, N. (2018). Lipid compound classes  
896 display diverging hydrogen isotope responses in lakes along a nutrient gradient.  
897 *Geochimica et Cosmochimica Acta*, 237, 103-119.  
898 <https://doi.org/10.1016/j.gca.2018.06.005>
- 899 Lee, H., Feakins, S. J., Lu, Z., Schimmelmann, A., Sessions, A. L., Tierney, J. E., Williams, T. J.  
900 (2017). Comparison of three methods for the methylation of aliphatic and aromatic  
901 compounds. *Rapid Communications in Mass Spectrometry*, 31, 1633-1640.  
902 <https://doi.org/10.1002/rcm.7947>
- 903 Leider, A., Hinrichs, K. -U., Schefuss, E., & Versteegh, G. J. M. (2013). Distribution and stable  
904 isotopes of plant wax derived n-alkanes in lacustrine, fluvial and marine surface sediments  
905 along an Eastern Italian transect and their potential to reconstruct the hydrological cycle.  
906 *Geochimica et Cosmochimica Acta*, 117, 16-32. <https://doi.org/10.1016/j.gca.2013.04.018>
- 907 Li C., Sessions A. L., Kinnaman F. S., & Valentine D. L. (2009). Hydrogen-isotopic variability  
908 in lipids from Santa Barbara Basin sediments. *Geochimica et Cosmochimica Acta*, 73,  
909 4803-4823. <https://doi.org/10.1016/j.gca.2009.05.056>
- 910 Li, Y., Yang, S., Luo, P., & Xiong, S. (2019). Aridity-controlled hydrogen isotope fractionation  
911 between soil n-alkanes and precipitation in China. *Organic Geochemistry*, 133, 53-64.  
912 <https://doi.org/10.1016/j.orggeochem.2019.04.009>
- 913 Linsley, B. K., Kaplan, A., Gouriou, Y., Salinger, J., DeMenocal, P., Wellington, G. M., &  
914 Howe, S. S. (2006). Tracking the extent of the South Pacific Convergence Zone since the  
915 early 1600s. *Geochemistry, Geophysics, and Geosystems*, 7, 1-15.  
916 <https://doi.org/10.1029/2005GC001115>
- 917 Linsley, B. K., Wellington, G. M., Schrag, D. P., Ren, L., Salinger, M. J., & Tudhope, A. W.  
918 (2004). Geochemical evidence from corals for changes in the amplitude and spatial pattern  
919 of South Pacific interdecadal climate variability over the last 300 years. *Climate Dynamics*,  
920 22, 1-11. <https://doi.org/10.1007/s00382-003-0364-y>
- 921 Liu, J., & An, Z. (2019). Variations in hydrogen isotope fractionation in higher plants and  
922 sediments across different latitudes: Implications for paleohydrological reconstruction.  
923 *Science of the Total Environment*, 650(1), 470-478.  
924 <https://doi.org/10.1016/j.scitotenv.2018.09.047>
- 925 Lu, J., Zang, J., Meyers, P., Huang, X., Qiu, P., Yu, X., et al. (2020). Surface soil n-alkane  
926 molecular and  $\delta D$  distributions along a precipitation transect in northeastern China.  
927 *Organic Geochemistry* 144, 104015. <https://doi.org/10.1016/j.orggeochem.2020.104015>
- 928 Maloney, A. E., Nelson, D. B., Richey, J. N., Prebble, M., Sear, D. A., Hassell, J. D., et al.  
929 (2019). Reconstructing precipitation in the tropical South Pacific from dinosterol  $^2H/^1H$   
930 ratios in lake sediment. *Geochimica et Cosmochimica Acta*, 245, 190-206.  
931 <https://doi.org/10.1016/j.gca.2018.10.028>
- 932 Maupin, C. R., Partin, J. W., Shen, C. -C., Quinn, T. M., Lin, K., Taylor, F. W., et al. (2014).  
933 Persistent decadal-scale rainfall variability in the tropical South Pacific Convergence Zone  
934 through the past six centuries. *Climate of the Past* 10, 1319-1332.  
935 <https://doi.org/10.5194/cp-10-1319-2014>
- 936 McFarlin, J. M., Axford, Y., Masterson, A. L., & Osburn, M. R. (2019). Calibration of modern  
937 sedimentary  $\delta^2H$  plant wax-water relationships in Greenland lakes. *Quaternary Science*  
938 *Reviews*, 225, 105978. <https://doi.org/10.1016/j.quascirev.2019.105978>
- 939 Meyers, P. A. (2003). Applications of organic geochemistry to paleolimnological  
940 reconstructions: a summary of examples from the Laurentian Great Lakes. *Organic*  
941 *Geochemistry*, 34(2), 261-289. [https://doi.org/10.1016/S0146-6380\(02\)00168-7](https://doi.org/10.1016/S0146-6380(02)00168-7)

- 942 Moore, P. D., Webb, J. A., & Collinson, M. E. (1991). Pollen analysis. Blackwell Scientific,  
943 Oxford.
- 944 Mueller-Dombois, D., & Fosberg, F. R. (1998). Vegetation of the tropical Pacific islands.  
945 Springer, New York.
- 946 Nelson, D. B., (2013). Hydrogen isotopes from lipid biomarkers: Purification, field calibration,  
947 and application to reconstructing Galapagos paleohydrology. University of Washington.
- 948 Nelson D. B., & Sachs J. P. (2016). Galápagos hydroclimate of the Common Era from paired  
949 microalgal and mangrove biomarker  $^2\text{H}/^1\text{H}$  values. *Proceedings of the National Academy*  
950 *of Sciences of the United States of America*, 113(13), 3476-3481.  
951 <https://doi.org/10.1073/pnas.1516271113>
- 952 Nelson, D. B., Knohl, A., Sachse, D., Schefuß, E., & Kahmen, A. (2017). Sources and  
953 abundances of leaf waxes in aerosols in central Europe. *Geochimica et Cosmochimica*  
954 *Acta*, 198, 299-314. <https://doi.org/10.1016/j.gca.2016.11.018>
- 955 Nelson, D. B., Ladd, S. N., Schubert, C. J., & Kahmen, A. (2018). Rapid atmospheric transport  
956 and large-scale deposition of recently synthesized plant waxes. *Geochimica et*  
957 *Cosmochimica Acta*, 222, 599-617. <https://doi.org/10.1016/j.gca.2017.11.018>
- 958 Newberry, S. L., Kahmen, A., Dennis, P., & Grant, A. (2015). *n*-Alkane biosynthetic hydrogen  
959 isotope fractionation is not constant throughout the growing season in the riparian tree  
960 *Salix viminalis*. *Geochimica et Cosmochimica Acta*, 165, 75-85.  
961 <https://doi.org/10.1016/j.gca.2015.05.001>
- 962 Newberry, S. L., Nelson, D. B., & Kahmen, A. (2017). Cryogenic vacuum artifacts do not affect  
963 plant water-uptake studies using stable isotope analysis. *Ecohydrology* 10:e1892.  
964 <https://doi.org/10.1002/eco.1892>
- 965 Osburn, M. R., Sessions, A. L., Pepe-Ranney, C., Spear, J. R. (2011). Hydrogen-isotopic  
966 variability in fatty acids from Yellowstone National Park hot spring microbial  
967 communities. *Geochimica et Cosmochimica Acta*, 75(17), 4830-4845.  
968 <https://doi.org/10.1016/j.gca.2011.05.038>
- 969 Partin, J. W., Quinn, T. M., Shen, C. -C., Emile-Geay, J., Taylor, F. W., Maupin, C. R., et al.  
970 (2013). Multidecadal rainfall variability in South Pacific Convergence Zone as revealed by  
971 stalagmite geochemistry. *Geology*, 41(11), 1143-1146. <https://doi.org/10.1130/G34718.1>
- 972 Peterse, F., van der Meer, M. T. J., Schouten, S., Jia, G., Ossebaar, J., Blokker, J., & Sinninghe  
973 Damste, J. S. (2009). Assessment of soil *n*-alkane  $\delta\text{D}$  and branched tetraether membrane  
974 lipid distributions as tools for paleoelevation reconstruction. *Biogeosciences*, 6, 2799-2807.
- 975 Prebble, M., & Wilmshurst, J.M. (2009). Detecting the initial impact of humans and introduced  
976 species on island environments in Remote Oceania using palaeoecology. *Biological*  
977 *Invasions*, 11, 1529–1556. <https://doi.org/10.1007/s10530-008-9405-0>
- 978 Prebble, M., Anderson, A. J., Augustinus, P., Emmitt, J., Fallon, S. J., Furey, L. L., et al. (2019).  
979 Early tropical Pacific production in marginal subtropical and temperate Polynesia.  
980 *Proceedings of the National Academy of Sciences of the United States of America* 116(18),  
981 8824-8833. <https://doi.org/10.1073/pnas.1821732116>
- 982 Polissar, P. J., & Freeman, K. H. (2010). Effects of aridity and vegetation on plant-wax  $\delta\text{D}$  in  
983 modern lake sediments. *Geochimica et Cosmochimica Acta*, 74(20), 5785-5797.  
984 <https://doi.org/10.1016/j.gca.2010.06.018>
- 985 Quinn, T. M., Crowley, T. J., Taylor, F. W., & Henin, C. (1998). A multicentury stable isotope  
986 record from a New Caledonia coral: interannual and decadal sea surface temperature  
987 variability in the Southwest Pacific since 1657 AD. *Paleoceanography*, 13(4), 412-426.  
988 <https://doi.org/10.1029/98PA00401>

- 989 Quinn, T. M., Taylor, F. W., & Crowley, T. J. (1993). A 173 year stable isotope record from a  
990 tropical South Pacific coral. *Quaternary Science Reviews*, 12(6), 407-418.  
991 [https://doi.org/10.1016/S0277-3791\(05\)80005-8](https://doi.org/10.1016/S0277-3791(05)80005-8)
- 992 Reef R., Markham H. L., Santini N. S., & Lovelock C. E., (2015). The response of the mangrove  
993 *Avicennia marina* to heterogeneous salinity measured using a split-root approach. *Plant*  
994 *Soil*, 393, 297–305. <https://doi.org/10.1007/s11104-015-2489-2>
- 995 Richey, J. N., & Sachs, J. P. (2016). Precipitation changes in the western tropical Pacific over the  
996 past millennium. *Geology*, 44(8), 671-674. <https://doi.org/10.1130/G37822.1>
- 997 Rozanski, K., Araguas-Araguas, L., & Gonfiantinin, R. (1993). Isotopic patterns in modern global  
998 precipitation. In P. K. Swart (Ed.) *Climate Change in Continental Isotopic Records*,  
999 *Volume 78* (pp. 1-36). Washington, DC: American Geophysical Union.  
1000 <https://doi.org/10.1029/GM078p0001>
- 1001 Sachs, J. P., Blois, J. L., McGee, T., Wolhowe, M., Haberle, S., Clark, G., Atahan, P. (2018).  
1002 Southward shift of the Pacific ITCZ during the Holocene. *Paleoceanography and*  
1003 *Paleoclimatology*, 33(12), 1383-1395. <https://doi.org/10.1029/2018PA003469>
- 1004 Sachs J. P., Sachse D., Smittenberg R. H., Zhang Z., Battisti D. S., & Golubic S. (2009).  
1005 Southward movement of the Pacific intertropical convergence zone AD 1400–1850. *Nature*  
1006 *Geoscience*, 2, 519–525. <https://doi.org/10.1038/NGEO554>
- 1007 Sachse, D., Billault, I., Bowen, G. J., Chikaraishi, Y., Dawson, T. E., Feakins, S. J., et al. (2012).  
1008 Molecular Paleohydrology: Interpreting the hydrogen-isotopic composition of lipid  
1009 biomarkers from photosynthesizing organisms. *Annual Review of Earth and Planetary*  
1010 *Sciences*, 40, 221–249. <https://doi.org/10.1146/annurev-earth-042711-105535>
- 1011 Sachse D., Radke J., & Gleixner G. (2004). Hydrogen isotope ratios of recent lacustrine  
1012 sedimentary n-alkanes record modern climate variability. *Geochimica et Cosmochimica*  
1013 *Acta*, 68(23), 4877-4889. <https://doi.org/10.1016/j.gca.2004.06.004>
- 1014 Santini N. S., Reef R., Lockington D. A., & Lovelock C. E. (2015). The use of fresh and saline  
1015 water sources by the mangrove *Avicennia marina*. *Hydrobiologia*, 745, 59–68.  
1016 <https://doi.org/10.1007/s10750-014-2091-2>
- 1017 Scholl, M. A., Giambelluca, T. W., Gingerich, S. B., Nullet, M. A., Loope, L. L. (2007). Cloud  
1018 water in windward and leeward mountain forests: The stable isotope signature of  
1019 orographic cloud water. *Water Resources Research*, 43, W12411.  
1020 <https://doi.org/10.1029/2007WR006011>
- 1021 Scholl, M. A., Ingebritsen, S. E., Janik, C. J., Kauahikaua, J. P. (1996). Use of precipitation and  
1022 groundwater isotopes to interpret region hydrology on a tropical volcanic island: Kilauea  
1023 volcano area, Hawaii. *Water Resources Research*, 32, 3525-3537.  
1024 <https://doi.org/10.1029/95WR02837>
- 1025 Schwab, V. F., Garcin, Y., Sachse, D., Todou, G., Sene, O., Onana, J. M., et al. (2015). Effect of  
1026 aridity on  $\delta^{13}\text{C}$  and  $\delta\text{D}$  values of C3 plant- and C4 graminoid-derived leaf wax lipids from  
1027 soils along an environmental gradient in Cameroon (Western Central Africa). *Organic*  
1028 *Geochemistry*, 78, 99-109. <https://doi.org/10.1016/j.orggeochem.2014.09.007>
- 1029 Sear, D. A., Allen, M. S., Hassall, J. D., Maloney, A. E., Langdon, P. G., Morrison, A. E., et al.  
1030 (2020). Human settlement of East Polynesia earlier, incremental, and coincident with  
1031 prolonged South Pacific drought. *Proceedings of the National Academy of Sciences of the*  
1032 *United States of America*, 117(16), 8813-8819. <https://doi.org/10.1073/pnas.1920975117>.
- 1033 Sharmila, S., & Walsh, K. J. E. (2018). Recent poleward shift of tropical cyclone formation  
1034 linked to Hadley cell expansion. *Nature Climate Change*, 8, 730-736.  
1035 <https://doi.org/10.1038/s41558-018-0227-5>

- 1036 Sichrowsky, U., Schabetsberger, R., Sonntag, B., Stoyneva, M., Maloney, A. E., Nelson, D. B.,  
1037 et al. (2014). Limnological characterization of volcanic crater lakes on Uvea Island (Wallis  
1038 and Futuna, South Pacific). *Pacific Science*, 68(3), 333-343. <https://doi.org/10.2984/68.3.3>
- 1039 Smittenberg R. H., Saenger C., Dawson M. N., & Sachs J. P. (2011). Compound-specific D/H  
1040 ratios of the marine lakes of Palau as proxies for West Pacific Warm Pool hydrologic  
1041 variability. *Quaternary Science Reviews*, 30(7-8), 921-933.  
1042 <https://doi.org/10.1016/j.quascirev.2011.01.012>
- 1043 Southern, W. (1986). The Late Quaternary Environmental History of Fiji. Australian National  
1044 University.
- 1045 Steen-Larsen, H. C., Risi, C., Werner, M., Yoshimura, K., Masson-Delmotte, V. (2017).  
1046 Evaluating the skills of isotope-enabled general circulation models against in situ  
1047 atmospheric water vapor isotope observations. *JGR Atmospheres*, 122(1), 246-263.  
1048 <https://doi.org/10.1002/2016JD025443>
- 1049 Stevenson, J., Dodson, J. R., & Prosser, I. P. (2001). A late Quaternary record of environmental  
1050 change and human impact from New Caledonia. *Palaeogeography, Palaeoclimatology,*  
1051 *Palaeoecology*, 168(1-2), 97-123. [https://doi.org/10.1016/S0031-0182\(00\)00251-0](https://doi.org/10.1016/S0031-0182(00)00251-0)
- 1052 Struck, J., Bliedtner, M., Strobel, P., Bittner, L., Bazarradnaa, E., Andreeva, D., et al. (2020).  
1053 Leaf waxes and hemicelluloses in topsoils reflect the  $\delta^2\text{H}$  and  $\delta^{18}\text{O}$  isotopic composition  
1054 of precipitation in Mongolia. *Frontiers in Earth Science*. 8:343.  
1055 <https://doi.org/10.3389/feart.2020.00343>
- 1056 Sturm, C., Zhang, Q., & Noone, D. (2010). An introduction to stable water isotopes in climate  
1057 models: Benefits of forward proxy modeling for paleoclimatology. *Climate of the Past*, 6,  
1058 115-129. <https://doi.org/10.5194/cpd-5-1697-2009>
- 1059 Tan, J., Jakob, C., Rossow, W. B., & Tselioudis, G. (2015). Increases in tropical rainfall driven  
1060 by changes in frequency of organized deep convection. *Nature*. 519, 451-454.  
1061 <https://doi.org/10.1038/nature14339>
- 1062 Terry, J. P. (2011). The Climate of Santo (Vanuatu). In P. Bouchet, H. Le Guyander, O. Pascal  
1063 (Eds.), *The Natural History of Santo* (pp. 52-56). Paris, France: Museum National  
1064 d'Histoire Naturelle.
- 1065 Tierney, J. E., deMenocal, P. B., & Zander, P. D. (2017). A climatic context for the out-of-Africa  
1066 migration. *Geology*, 45 (11): 1023-1026. <https://doi.org/10.1130/G39457.1>
- 1067 Tipple B. J., Berke M. A., Doman C. E., Khachatryan S., & Ehleringer J. R. (2013). Leaf *n*-  
1068 alkanes record the plant-water environment at leaf flush. *Proceedings of the National*  
1069 *Academy of Sciences of the United States of America* 110(7), 2659-2664.  
1070 <https://doi.org/10.1073/pnas.1213875110>
- 1071 Tipple, B. J., Berke M. A., Hambach B., Roden J. S., & Ehleringer J. R. (2015). Predicting leaf  
1072 wax *n*-alkane  $^2\text{H}/^1\text{H}$  ratios: Controlled water source and humidity experiments with  
1073 hydroponically grown trees confirm predictions of Craig-Gordon model. *Plant, Cell and*  
1074 *Environment*, 38(6), 1035-1047. <https://doi.org/10.1111/pce.12457>
- 1075 van Bree, L. G. J., Peterse, F., van der Meer, M. T. J., Middelburg, J. J., Negash, A. M. D., De  
1076 Crop, W., et al. (2018). Seasonal variability in the abundance and stable carbon-isotopic  
1077 composition of lipid biomarkers in suspended particulate matter from a stratified  
1078 equatorial lake (Lake Chala, Kenya/Tanzania): Implications for the sedimentary record.  
1079 *Quaternary Science Reviews*, 192, 208-224.  
1080 <https://doi.org/10.1016/j.quascirev.2018.05.023>
- 1081 van der Veen, I., Peterse, F., Davenport, J., Meese, B., Bookhagen, B., France-Lanord, C., et al.  
1082 (2020). Validation and calibration of soil  $\delta^2\text{H}$  and brGDGTs along (E-W) and strike (N-S)

1083 of the Himalayan climatic gradient. *Geochimica et Cosmochimica Acta*.  
1084 <https://doi.org/10.1016/j.gca.2020.09.014>

1085 Volkman J. K. (2003). Sterols in microorganisms. *Applied Microbiology and Biotechnology*, 60,  
1086 495–506. <https://doi.org/10.1007/s00253-002-1172-8>

1087 Volkman J. K., Johns R. B., Gillian, F. T., & Perry G. J. (1980). Microbial lipids of an intertidal  
1088 sediment – I. Fatty acids and hydrocarbons. *Geochimica et Cosmochimica Acta*, 44(8),  
1089 1133-1143. [https://doi.org/10.1016/0016-7037\(80\)90067-8](https://doi.org/10.1016/0016-7037(80)90067-8)

1090 Wu, M. S., West, A. J., & Feakins, S. J. (2019). Tropical soil profiles reveal the fate of plant wax  
1091 biomarkers during soil storage. *Organic Geochemistry*, 128, 1-15.  
1092 <https://doi.org/10.1016/j.orggeochem.2018.12.011>

1093 Yoshimura, K., Kanamitsu, M., Noone, D., & Oki, T. (2018). Historical isotope simulation using  
1094 reanalysis atmospheric data. *Journal of Geophysical Research: Atmospheres*, 113(D19),  
1095 D19108. <https://doi.org/10.1029/2008JD010074>

1096 Zhang X., Gillespie A., & Sessions A. L. (2009). Large D/H variations in bacterial lipids reflect  
1097 central metabolic pathways. *Proceedings of the National Academy of Sciences of the*  
1098 *United States of America*, 106(31), 12580-12586. <https://doi.org/10.1073/pnas.0903030106>

1099 Zhang Z., & Sachs J. P. (2007). Hydrogen isotope fractionation in freshwater algae: 1. Variations  
1100 among lipids and species. *Organic Geochemistry*, 38(4), 582–608.  
1101 <https://doi.org/10.1016/j.orggeochem.2006.12.004>

1102  
1103  
1104  
1105  
1106  
1107  
1108  
1109  
1110  
1111  
1112  
1113  
1114  
1115  
1116  
1117  
1118  
1119  
1120  
1121  
1122  
1123  
1124  
1125  
1126  
1127  
1128  
1129  
1130  
1131  
1132  
1133  
1134

1135 **Table 1** Lake location, total number of samples analyzed per site,  $\delta^2\text{H}$  values of local precipitation and  
 1136 leaf waxes, and measured  $\delta^2\text{H}_{\text{Wax}}$  values with residuals from predicted values based on linear correlation  
 1137 of compiled literature values

Site, Island, Country	Lat. ( $^{\circ}\text{N}$ ) <sup>1</sup>	Long. ( $^{\circ}\text{E}$ ) <sup>1</sup>	# of samples	$\delta^2\text{H}_{\text{P}}$ ( $\text{‰}$ , VSMOW) <sup>2</sup>	$\delta^2\text{H } n\text{-C}_{29}$ alkane <sup>3</sup> (residual from global relationship <sup>4</sup> ) ( $\text{‰}$ , VSMOW)	$\delta^2\text{H } n\text{-C}_{28}$ acid <sup>3</sup> (residual from global relationship <sup>4</sup> ) ( $\text{‰}$ , VSMOW)
<b>Lakes</b>						
Rimatu'u Pond, Tetiaroa, French Polynesia	-17.0249	210.4417	2	-25 ± 26	-177 (-38 ± 12)	-160 ± 17 (-28 ± 19)
Oroatera Pond, Tetiaroa, French Polynesia	-16.9958	210.4591	1	-25 ± 26	-173 (-34 ± 12)	N.A.
Onetahi Pond, Tetiaroa, French Polynesia <sup>#</sup>	-17.0207	210.4081	1	-25 ± 26	-139 (-0 ± 12)	-126 (5 ± 10)
Lake Lanoto'o, Upolu, Samoa	-13.9109	188.1726	3	-34 ± 3	-159 (-12 ± 1)	-148 ± 6 (-9 ± 6)
Lac Lalolalo, Wallis, Wallis and Futuna	-13.3017	183.7662	3	-23 ± 1	N.A.	-150 ± 6 (-20 ± 6)
Lac Lanutavake, Wallis, Wallis and Futuna	-13.3212	183.7860	2	-24 ± 2	N.A.	-140 ± 9 (-9 ± 9)
Lake Dranoniveilomo, Vanua Balavu, Fiji	-17.1976	181.0441	2	-21 ± 11	-151 (-15 ± 5)	-173 ± 14 (-44 ± 14)
Lake Tagamaucia, Teveuni, Fiji <sup>#</sup>	-16.8163	180.0601	2	-34 ± 14	-170 ± 1 (-23 ± 7)	-175 ± 1 (-36 ± 5)
Otas Lake, Efate, Vanuatu	-17.6945	168.5850	1	-34 ± 73	-154 (-6 ± 35)	-136 (2 ± 27)
Emaotul Lake, Efate, Vanuatu	-17.7342	168.4151	3	-36 ± 76	-152 ± 9 (-3 ± 36)	-130 ± 3 (9 ± 26)
White Lake, Thion, Vanuatu	-15.0410	167.0892	2	-35 ± 70	-174 (-25 ± 34)	-119 ± 2 (21 ± 26)
Waérowa East Lake, Espiritu Santo, Vanuatu <sup>#</sup>	-15.5950	167.0788	1	-34 ± 71	N.A.	-155 (-16 ± 27)
Nopovois Pond, Espiritu Santo, Vanuatu	-15.4970	166.7357	1	-40 ± 71	-154 (-1 ± 34)	-122 (21 ± 27)
Vesalea Pond, Espiritu Santo, Vanuatu <sup>#</sup>	-15.1589	166.6549	1	-40 ± 70	-157 (-4 ± 34)	N.A.
Lake Hut, Grande Terre, New Caledonia	-22.2609	166.9526	2	-15 ± 54	-161 ± 2 (-31 ± 26)	-133 ± 1 (-8 ± 20)
Lake Tavara, Tetepare, Solomon Islands	-8.7029	157.4503	1	-46 ± 43	-162 (-4 ± 21)	-156 (-9 ± 16)
Lake Rano, Rendova, Solomon Islands	-8.6879	157.3243	2	-47 ± 42	N.A.	-135 ± 5 (13 ± 17)
Harai Lake #1, Rendova, Solomon Islands	-8.5622	157.3556	1	-47 ± 42	N.A.	-121 (27 ± 16)
Harai Lake #3, Rendova, Solomon Islands	-8.5648	157.3651	2	-47 ± 42	N.A.	-134 ± 11 (15 ± 19)
<b>Mangrove swamps</b>						
Sapwalap Swamp, Pohnpei, Fed. States of Micronesia	6.88	158.30	5	-33 ± 2	-150 ± 5 (-3 ± 5)	N.M.
Tol Swamp, Chuuk, Fed. States of Micronesia	7.35	150.60	4	-32 ± 1	-153 ± 5 (-2 ± 5)	N.M.
Sasa Swamp, Guam, United States	13.45	140.73	4	-29 ± 1	-145 ± 5 (-7 ± 5)	N.M.
Galal Swamp, Yap, Fed. States of Micronesia	9.50	138.08	5	-34 ± 1	-151 ± 6 (-3 ± 6)	N.M.

1138  
 1139 <sup>1</sup>Less precision is provided for latitude and longitude in mangrove swamps because swamp samples were collected  
 1140 along a transect typically spanning > 1 km.

1141 <sup>2</sup>Mean annual precipitation  $\delta^2\text{H}$  values (relative to VSMOW) from OIPC ± 95% confidence intervals.

1142 <sup>3</sup>Mean value of multiple surface sediment measurements from same lake, relative to VSMOW. Uncertainties  
1143 represent 1 standard deviation. When only one sample was analyzed no uncertainty is reported. Analytical  
1144 uncertainty for compound specific  $\delta^2\text{H}$  measurements is 4‰. “*N.A.*” = compound was not present or was below  
1145 detection limit for  $\delta^2\text{H}$  measurements. “*N.M.*” = not measured.

1146 <sup>4</sup>Residuals are offsets from global calibration line of compiled leaf wax  $\delta^2\text{H}$  values from the literature. Uncertainties  
1147 are site specific standard deviations of OIPC  $\delta^2\text{H}$  values, and are propagated with standard deviations of leaf wax  
1148  $\delta^2\text{H}$  values when multiple samples are available from a site.

1149 <sup>#</sup>Lakes with greater than 50% vegetation cover

1150  
1151  
1152  
1153  
1154  
1155  
1156  
1157  
1158  
1159  
1160  
1161  
1162  
1163  
1164  
1165  
1166  
1167  
1168  
1169  
1170  
1171  
1172  
1173  
1174  
1175  
1176  
1177  
1178  
1179  
1180  
1181  
1182  
1183  
1184  
1185  
1186  
1187  
1188  
1189  
1190  
1191  
1192

1193 **Table 2** Pollen counts from near surface sediments, reported as a percentage of total palynomorphs counted. For each sediment sample, age ranges  
 1194 are presented for the top and bottom depth.

Site, Island, Country	Depth of pollen sample (cm)	Bacon age at top of interval (year C.E.) <sup>\$</sup>	Bacon age at bottom of interval (year C.E.) <sup>\$</sup>	Primary forest (%)	Secondary forest (%)	Mangroves (%)	Ferns (%)	Non-vascular plants (%)	Dryland herbs (%)	Wetland herbs (%)	Aquatic plants (%)	Unknown (%)
Lake Lanoto'o, Upolu, Samoa	1-2	2013 ± 1	2002 ± 1	3.0	24.6	0	62.8	0	2.7	6.9	0	0
Lac Lalolalo, Wallis, Wallis and Futuna*	1-3	2001 +8 -14	1991 + 14 -19	10.3	57.1	0	16.4	0	0.4	13.4	0.8	1.7
Lac Lanutavake, Wallis, Wallis and Futuna	3-4	1990 +20 -64	1983 +26 -86	13.1	69.1	0	4.3	0	6.2	4.6	0	2.7
Lake Dranoniveilomo, Vanua Balavu, Fiji	2-3	2010 ± 2	2009 ± 3	21.0	33.6	0.7	17.5	1.4	4.2	19.6	0	2.1
Lake Tagamaucia, Teveuni, Fiji#	2-3	1989 ± 7	1978 ± 10	5.1	13.4	0	58.6	0	0.6	21.3	0	1.0
Otas Lake, Efate, Vanuatu	2-3	N.A.	N.A.	4.7	52.1	15.6	2.7	0	0	21.8	0.8	2.3
Emaotul Lake, Efate, Vanuatu	1-2	2016 ± 3.4	2014 ± 3.4	4.9	55.8	0	12.7	0.3	11.4	8.4	5.2	1.3
White Lake, Thion, Vanuatu	3-4	1997 +23 -14	1991 +30 -19	1.3	42.3	0	39.3	0	2.1	11.7	0	3.4
Waérowa East Lake, Espiritu Santo, Vanuatu#	3-1	2010 ± 3	2009 ± 3	1.2	11.2	14.1	35.9	0	11.2	14.7	7.7	4.1
Nopovois Pond, Espiritu Santo, Vanuatu	0-1	2017	N.A.	16.3	53.5	0	15.0	0	8.9	3.1	0.3	2.6
Vesalea Pond, Espiritu Santo, Vanuatu#	0-1	2016 +1 -3	2005 +10 -14	6.5	46.2	0	18.8	1.5	11.4	6.8	4.6	4.3
Lac Hut, Grand Terre, New Caledonia	0-1	N.A.	N.A.	50.1	41.1	0	4.8	0	0	0.9	0	3.1
Lake Tavara, Tetepare, Solomon Islands	8-9	1996 ± 5	1993 ± 6	6.3	23.4	6.3	54.7	0	1.6	7.8	0	0.1
Lake Rano, Rendova, Solomon Islands	9-10	1969 +17 -16	1960 +21 -20	16.7	46.5	0	29.8	0	0	4.4	0.9	1.8
Harai Lake #1, Rendova, Solomon Islands	11-12	1716 +99 -123	1702 +103 -120	5.4	19.4	2.2	66.7	0	0	5.4	0	1.1
Harai Lake #3, Rendova, Solomon Islands	30-31	1871 ± 85	1866 +86 -84	3.1	5.2	0	91.8	0	0	0	0	0

1195 \*Mean of 2 samples from different sites in these lakes. Age ranges presented represented the mean age for the top and bottom of each interval, and  
 1196 the full range of possible ages for both sites.

1197 # Lakes with greater than 50% vegetation cover

1198 \$ Age ranges are provided from sites with existing age models, the details of which are provided by Maloney et al. (2019), Krentscher et al. (2019),  
 1199 Gosling et al. (2020), and Sear et al. (2020)

1200

1201

1202

Figure 1.

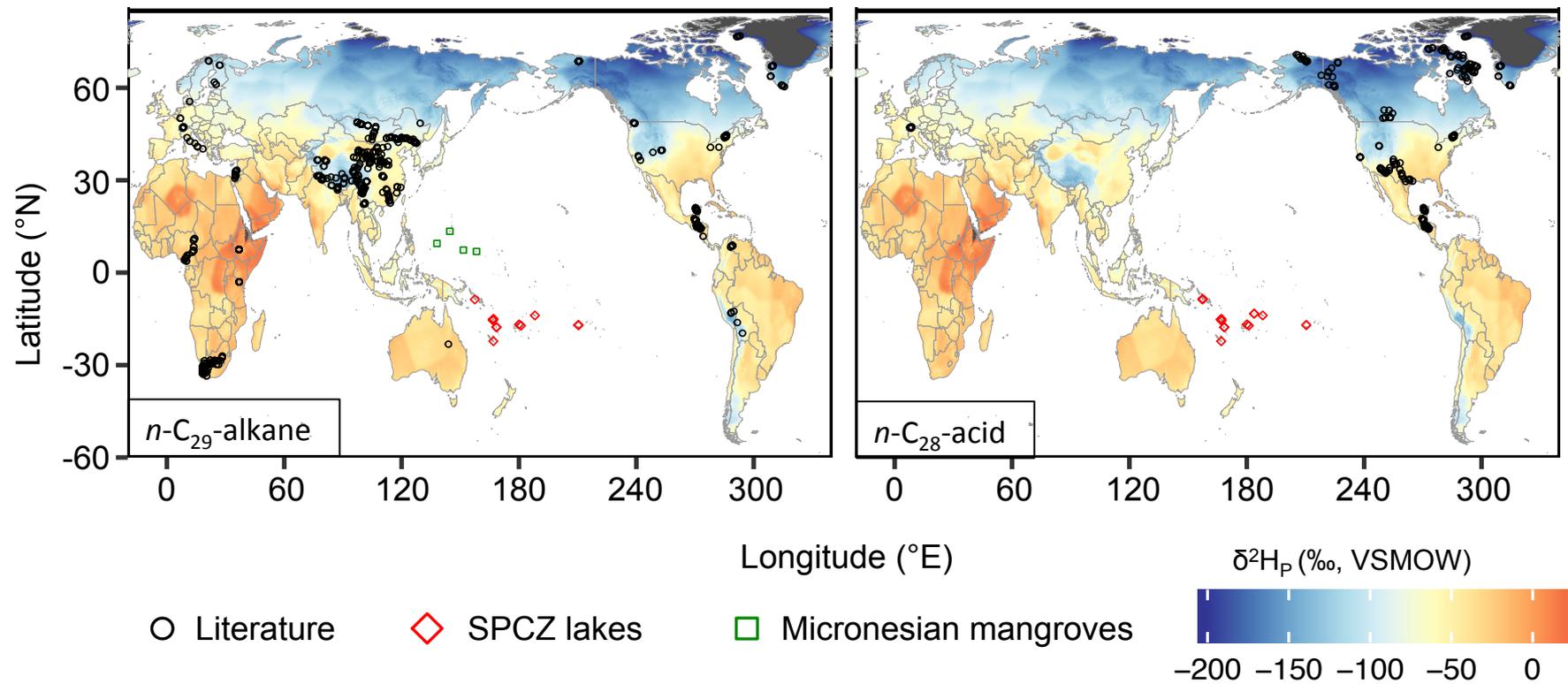


Figure 2.

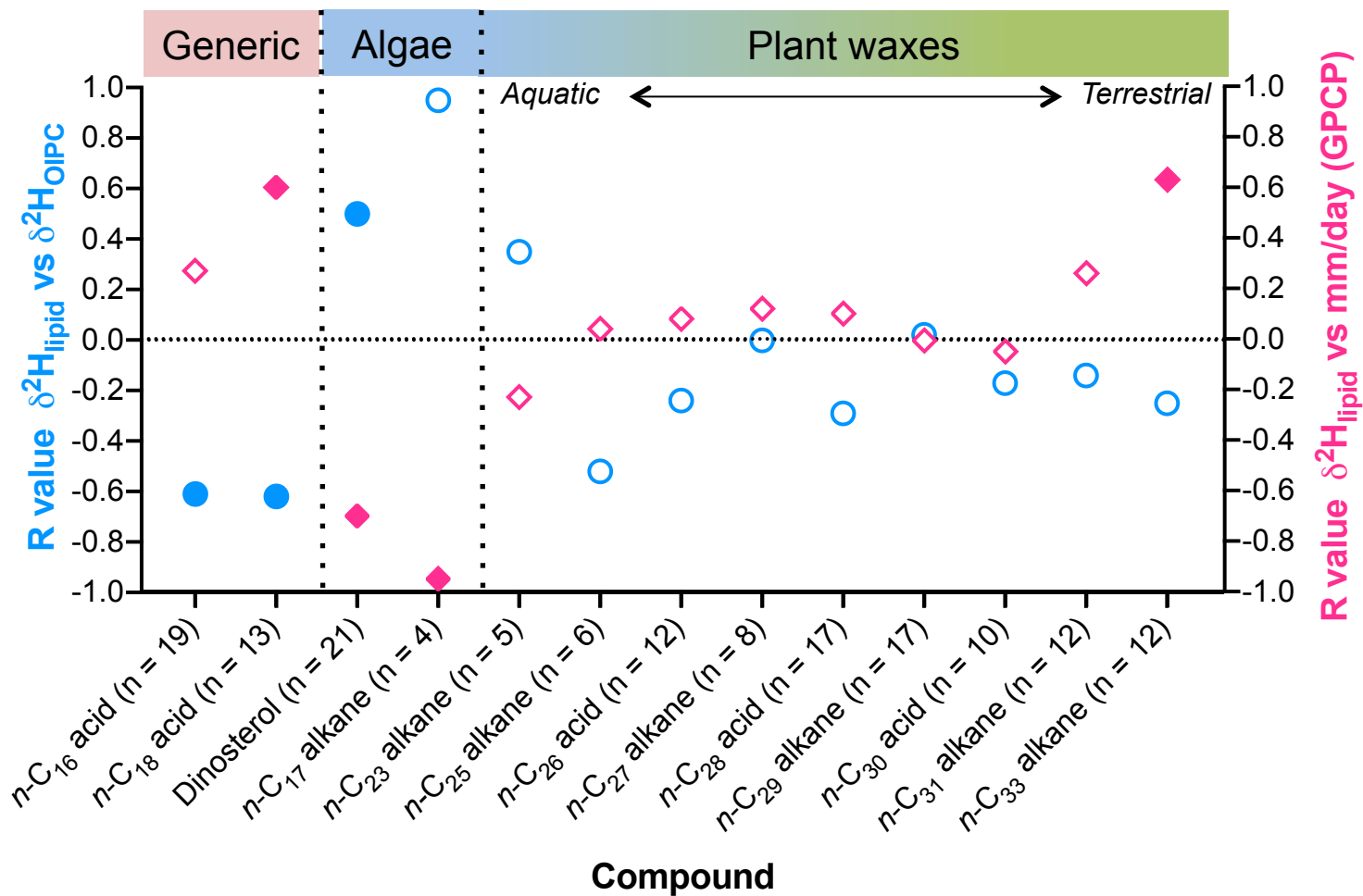
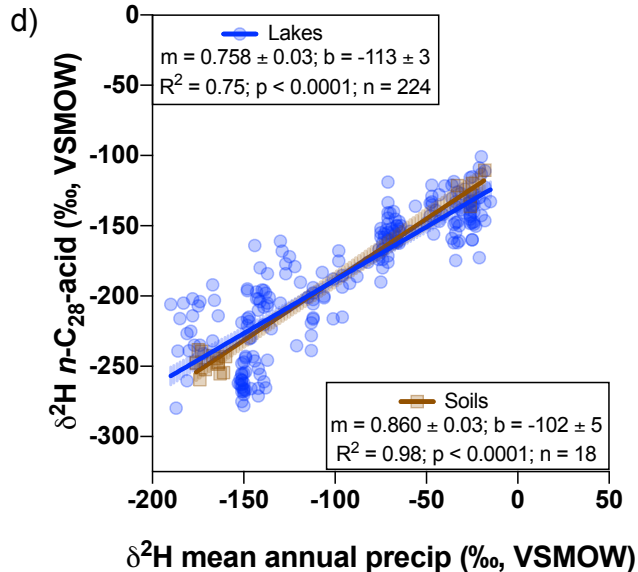
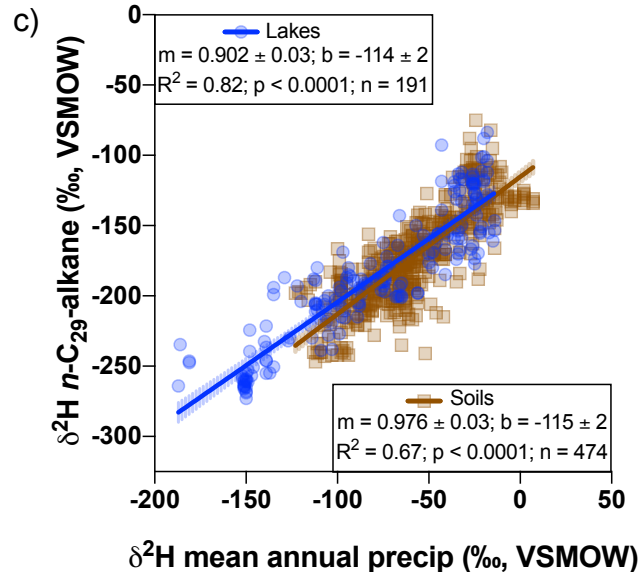
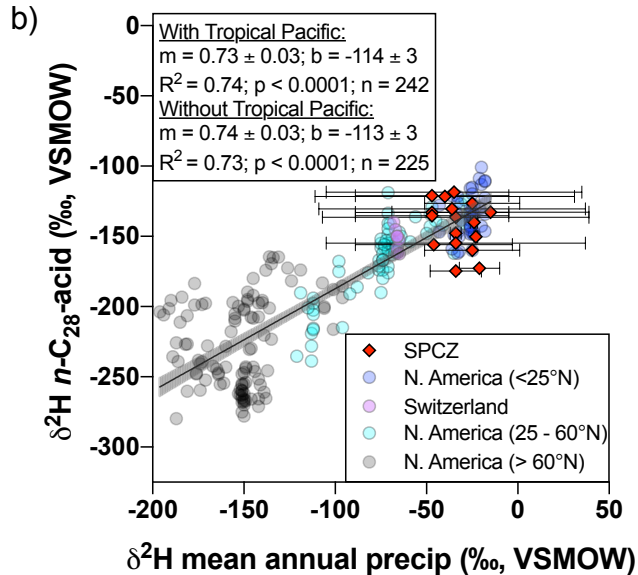
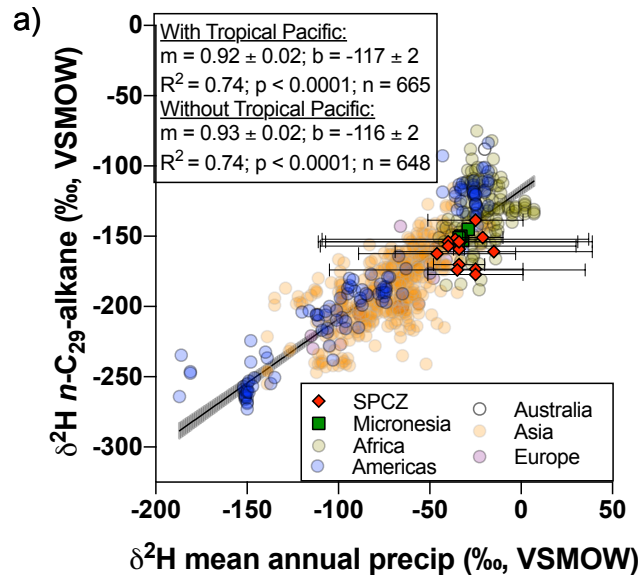


Figure 3.



**Figure 4.**

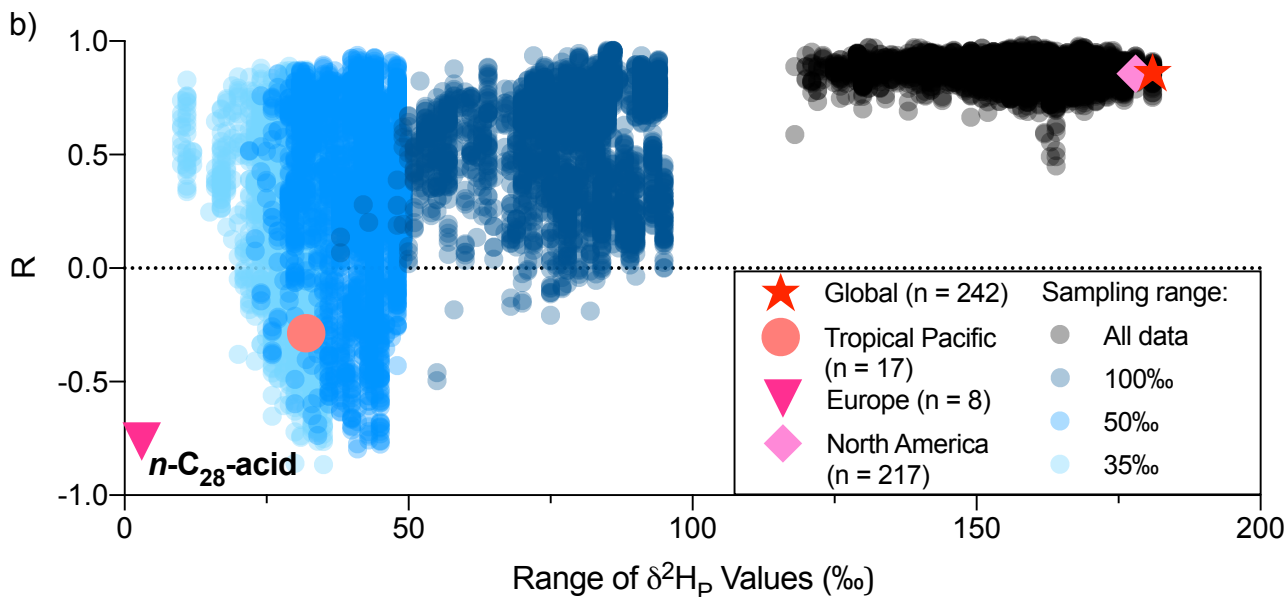
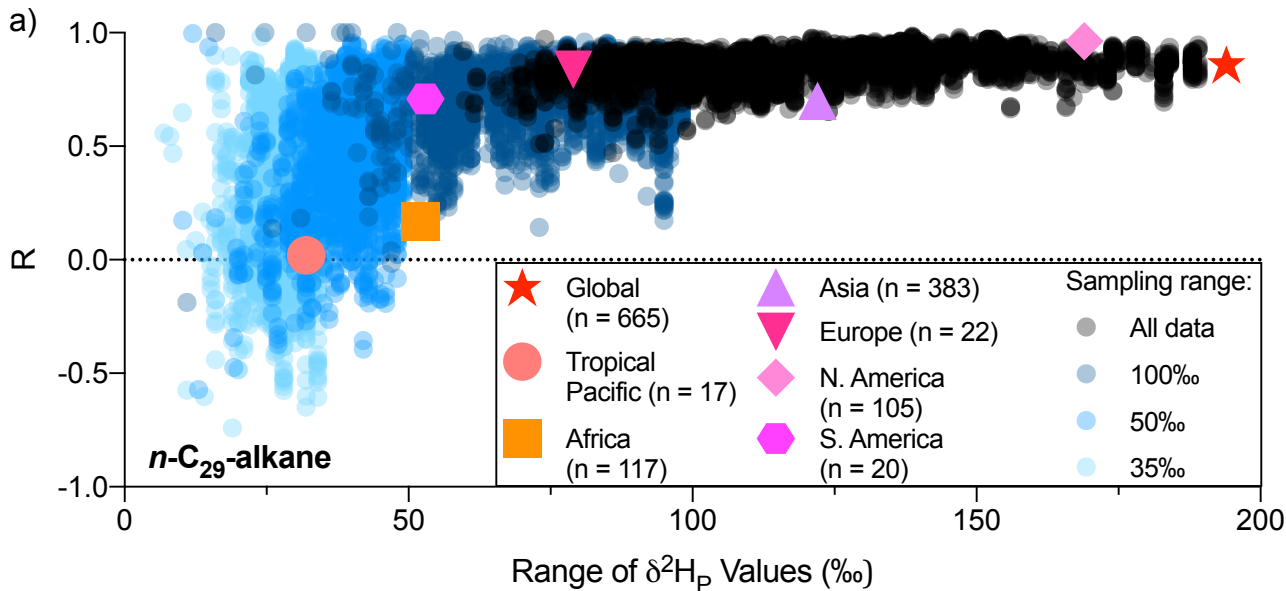


Figure 5.

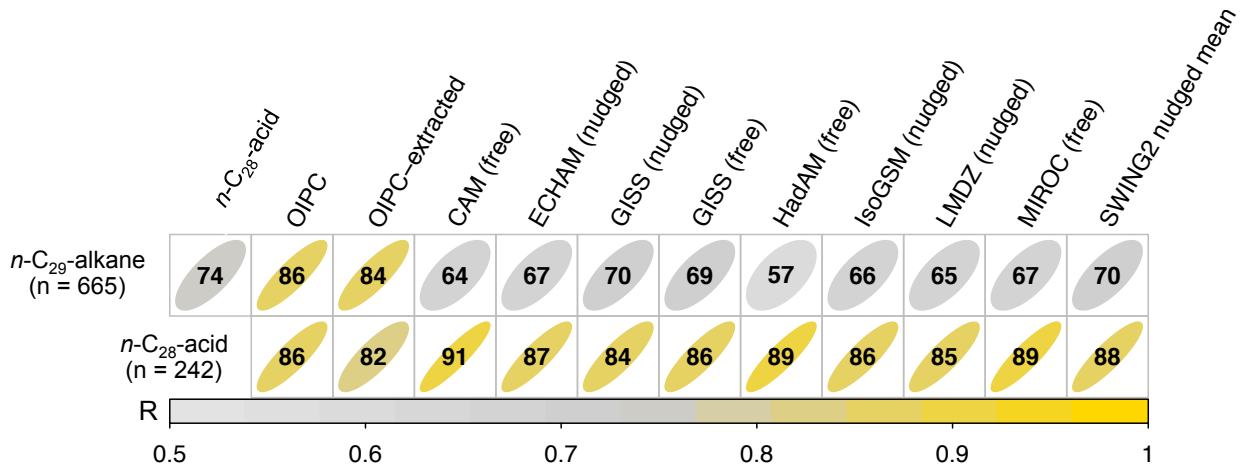


Figure 6.

